Highlights

Technoeconomic Assessment of Solar Technologies for the Hybridization of Industrial Process Heat Systems Using Deterministic Global Dynamic Optimization[⋆]

Justin Rastinejad, Sloane Putnam, Matthew D. Stuber

- New models are developed for global dynamic optimization of solar process heat
- Optimal designs are found for three geographic locations and five system options
- Parabolic trough collectors outperform PV in both efficiency and economics
- Battery electric storage technologies are economically infeasible for process heat

Technoeconomic Assessment of Solar Technologies for the Hybridization of Industrial Process Heat Systems Using Deterministic Global Dynamic Optimization

Justin Rastinejad[a,1,**], Sloane Putnam[a,2,**], Matthew D. Stuber[a,*]

[a]*Process Systems and Operations Research Laboratory, Department of Chemical and Biomolecular Engineering, University of Connecticut, Storrs, 06269-3222, Connecticut, USA*

Abstract

The industrial process heat (IPH) sector provides an opportunity to replace terawatts of fossil fuel energy with solar alternatives, such as parabolic trough collectors (PTC) or photovoltaics (PV) with resistive heating and energy storage (ES) for off-peak deployment. PTCs offer significantly higher thermal efficiency, but have stagnated in cost and efficiency improvements over the past decade. In contrast, PVs have seen significant improvements in cost and efficiency. Additionally, the energy generated by PV can be stored electrochemically in batteries. Current optimization-based approaches for design and investment decision making lack guarantees of global optimality that are necessary to ensure the best-possible solutions are obtained for these general nonconvex dynamical models. We present dynamical models for the formal deterministic global optimization-based design and technoeconomic assessment of solar systems to hybridize IPH and reduce natural gas combustion

*Author's final accepted version. Published version: Rastinejad, J., Putnam, S., and Stuber, M.D. Technoeconomic assessment of solar technologies for the hybridization of industrial process heat systems using deterministic global dynamic optimization. *Renewable Energy* (2023) doi:10.1016/j.renene.2023.119069

*Corresponding author.

**Authors share co-first authorship.

Email address: stuber@alum.mit.edu (Matthew D. Stuber)

[1]Current address: University of California Berkeley, Department of Chemical & Biomolecular Engineering, Berkeley, CA, 94720, USA

[2]Current address: Universitat Rovira i Virgili, School of Chemical Engineering, 43003 Tarragona, Spain

that serve as a general and flexible framework. We compare hybridization strategies of PTC with thermal ES, PV with thermal ES, and PV with battery ES and explore the impacts of natural gas pricing and process scale. For the low- to medium-temperature IPH, PTC with thermal ES is currently at least four times more economically favorable than alternative technologies regardless of location or process scale.

Keywords: deterministic global optimization, greenhouse gas reduction, sustainable manufacturing, decarbonization, solar energy storage, solar system design
2020 MSC: 90C30, 90C90, 37N40

---

1. Introduction

1.1. Background and Motivation

To mitigate the effects of climate change, it is imperative to reduce the dependence of humanity on CO_2-emitting processes. In 2019, fossil fuels represented almost 80% of the energy production of the United States, which totaled 100 quadrillion BTU (quads) [1]. In 2021, the industrial sector consumed more than 22 quads, with 20.4 quads produced by fossil fuels [2]. The combined production of solar, wind, geothermal, and hydro technologies only accounts for 48 trillion BTU; three orders of magnitude less than fossil fuels [2]. In the industrial sector, approximately 7.5 quads are consumed for industrial process heat (IPH) annually [3].

IPH is a diverse category of energy that encompasses the processing and manufacturing of products under wide-ranging temperature conditions. In Europe, low temperature IPH ($\leq$100 °C) accounted for 30% of the total IPH energy demand [4]. In the US, 60% of IPH energy demand was below 300 °C in 2015 [4, 5]. Industries that use these low temperatures include food and beverages, textiles, paper and pulp, and plastics [4]. Almost all of this heat is provided by burning fossil fuels [2]. To reduce our carbon footprint, researchers have explored more sustainable options. However, the most economical and practical method has not yet been identified.

To better complement the increasing energy generation from renewable sources, researchers have begun to explore the electrification of low-temperature IPH [6]. Electrification of an industry is the process of shifting to electrical energy usage from a nonelectrical source, such as fossil fuels. Globally, electricity use in industry has risen from 24.8% in 2000 to 28.5% in 2019,

corresponding to an increase of 40 quads over that time span [7]. Madeddu et al. [8] explored the feasibility of electrification for IPH in Europe and identified sectors where it can be feasible. If widely adopted, electrification could reduce CO_2 emissions by 78% by 2050 if the energy sector continues to decarbonize [8]. Hasanbeigi et al. [5] investigated the electrification potential of 13 sectors in the US and found that the steel and ammonia industries have the greatest potential to reduce CO_2 emissions if they are electrified. If these 13 sectors were decarbonized, the authors estimate that emissions would decrease by 134 million tonnes of CO_2 equivalent in 2050 [5].

The electrification of industrial processes also has many benefits for companies. For example, the generation of electricity on site protects companies from the volatility of natural gas prices [9]. Furthermore, electrified processes do not create air pollutants, leading to improved air quality compared to natural gas processes. Electrically powered heaters have also been shown to outperform their natural gas counterparts. For example, some electric boilers have 40% lower capital costs than their natural gas-powered counterparts [5]. Electrically powered heaters may also be more thermally efficient than traditional boilers, as in the case of vapor compression heat pumps [8].

Solar energy generation is expected to expand and improve to meet the demands of electrification. Photovoltaic (PV) panel production increased 56% every year on average between 2005 and 2012 [10]. In 2020 alone, 15 gigawatts of PV power were installed [11]. The US Solar Energy Technologies Office (SETO) expects solar PV installation to reach 1 terawatt by 2035, representing 30-50% of all US energy production [11]. This increase in usage will encourage additional investment and research, which is expected to drive the cost of PV energy even lower.

PV technologies have experienced significant price reductions in the last decade driven by investments from governments and industry [10]. Germany invested €53 billion between 2000 and 2010, and the state of California invested US$2.16 billion from 2007 to 2016 [10]. These subsidies have worked, as one study found that the stimulated market represented 60% of the price reduction [12]. Increased research on production has reduced the cost of PV energy to a quarter of the price that it was in 2008 [10]. The reduction in PV prices were driven by an increase in efficiency and a reduction in the cost of polysilicon [10].

However, this industrial shift towards electrification comes with consequences. Despite recent advocacy for electrification, electricity rates are still 2-14 times higher than natural gas rates [6]. A case study focusing on an oil

refinery found that electrifying the process is three to four times more expensive than natural gas alternatives [13]. Furthermore, electrified processes require new equipment, leading to high upfront costs [9]. The heterogeneity of IPH requires the creation of different types of heaters, each suited for the demands of specific processes. This variation removes the ease of production that would otherwise drive down prices.

On-site solar thermal technologies provide an equally sustainable alternative to electrification. Solar thermal technologies are responsible for 7 GW of global energy generation from almost 100 different sites [14]. Of particular interest in this study are parabolic trough collectors (PTCs), which use reflective mirrors to concentrate the sun's rays to heat a working fluid to high temperatures. Depending on their size, PTCs can achieve temperatures up to 400°C [4, 15, 16]. PTCs require at least 1-axis tracking systems for continuous operation, typically aligned North-South with East-West tracking [15, 16]. The economic feasibility of PTCs for IPH has been thoroughly investigated [15, 16, 17]. However, due to the significant decrease in natural gas costs in the last 14 years, much of this technology has stagnated in development [18]. Despite this, researchers and practitioners agree that PTCs are economically viable and important technologies for reducing carbon emissions in certain IPH sectors.

1.2. Optimization-Based Technoeconomic Assessment of Solar Hybridization

Optimization has been an important tool for analyzing solar thermal energy system hybridization, and various approaches have emerged in the last few years. A notable development by Powell et al. [19] focused on hybridizing fossil fuel energy systems using PTCs coupled to thermal energy storage (TES) systems. High-fidelity spatiotemporal heat transfer models were employed to model fluid temperatures in the PTC-TES system under transient operation [19]. A dynamic optimization problem was formulated to determine the control of PTC-TES heat transfer fluid flowrates that minimize overall pumping requirements and supplementary fossil fuel consumption [19]. An orthogonal collocation numerical integration approach was applied to discretize the model into algebraic equations, and the optimization problem was solved to local optimality, presumably with IPOPT [20]. Their findings helped to significantly increase solar utilization on partly cloudy days. However, their analysis only considered the optimal control of the PTC-TES system and, as such, accounted for the operating costs/savings and did not

consider the economic viability of these systems designs with respect to capital investment [19]. Furthermore, global optimality was not guaranteed.

Allouhi et al. [21] studied the solar hybridization of low-temperature thermal processes with flat-plate collectors with application to milk processing in Morocco. High-fidelity spatiotemporal heat transfer models were employed and solved using the TRANSOL simulator. Both the annual lifecycle cost and annual lifecycle savings were considered in their analysis and the annual lifecycle savings was considered as the economic objective function of their optimization formulation with tilt angle, aperture area, and storage capacity as the optimization variables [21]. However, the authors describe a one-factor-at-a-time procedure for determining a "good" design without any formal mathematical optimization and, as a result, no guarantees of optimality. Such one-factor-at-a-time approaches are inadequate for investment decision making involving nonlinear and nonconvex models.

Another low-temperature flat-plate solar thermal system was considered by Scolan et al. [22] to supply heat as a utility. Since the perspective was on optimizing operations, high-fidelity dynamical heat transfer models were considered with spatial dependence in the TES model [22]. Similar to Powell et al. [19], a formal dynamic optimization approach was applied to determine the optimal heat transfer fluid flowrates that result in the optimal economics (overall profit in this case) [22]. The same solution method of Powell et al. [19] was used, except that the discretized algebraic equations were then implemented in GAMS [23] and solved to local optimality using CONOPT [24]. Their optimized results reduced electricity consumption by 60% and increased economic profits by 2% [22].

In 2022, Immonen and Powell [25] continued development of the approach of Powell et al. [19] to improve controls (applying a hierarchical approach) for flexible heat integration to provide IPH for two separate processes. A more detailed high-fidelity spatiotemporal heat transfer model of the PTC-TES system was used that accounted for the heat exchangers for the two upstream IPH systems [25]. A dynamic optimization problem was formulated with an operational performance-based objective to maximize daily solar energy utilization with respect to hourly control actions (i.e., heat transfer fluid flowrates) [25]. Although the focus was on operations, an economic analysis was also applied using a metric of the levelized cost of heat that accounted for fixed (linear) capital pricing [25]. A simulation-based approach was applied to numerically integrate the spatially-discretized dynamical models and the dynamic optimization problems were solved using the particle-swarm meta-

heuristic algorithm [25]. As such, the optimization approach is only guaranteed to approximate a local minimum in the best case and, in the worst case, may not converge at all [26].

In 2018, a hybrid solar thermal/natural gas system for IPH was studied [17] based on dynamic heat flux models. The process considered PTCs for thermal power generation and gravel-packed bed tanks for TES. A new dynamic optimization-based design model was developed for more rigorous technoeconomic analyses and investment decision making with respect to solar hybridization and accounted for more accurate nonconvex economic models. In that work, a technoeconomic analysis was conducted for three disparate locations of the United States and the economic feasibility was assessed based on the power demand and constraints of the system, as well as the capital costs required [17]. The dynamic optimization problem was solved to guaranteed global optimality using a novel deterministic global optimization approach [17]. However, like the previous dynamic optimization work in this area, Stuber [17] did not consider alternative solar hybridization strategies for IPH, such as electrification approaches, and therefore, the technoeconomic analyses were limited.

Currently, there are few models that compare the economic feasibility of PV and resistive heating with concentrating solar thermal for IPH applications. In 2018, Meyers et al. [27] created a model in TRNSYS to compare the economic feasibility of solar thermal versus PV technologies. Their analysis determined that solar thermal energy outperformed PVs for almost all applications and found the exact prices that needed to be met for the technologies to become economically viable [27]. However, their analysis did not include hybridization strategies and instead focused on the energy price parity metric. Thus, their system only used solar power and could not consider variable-demand profiles and optimal system sizing. Mousa et al. [28] used TRNSYS and explored the optimal sizes of systems hybridized with natural gas, PTCs, and PVs for various global locations. Their results found that combining PVs with PTCs could dramatically improve the levelized cost of energy over only using PTCs, which highlights the viability of PVs for the production of IPH [28].

While TRNSYS is a popular and powerful dynamic simulation software tool used for modeling solar energy systems, it is not capable of deterministic global optimization. Current optimization techniques for TRNSYS include data-driven artificial neural network-based approaches, which are computationally expensive to train, or GenOPT, which is a derivative-free blackbox

optimizer and as such, cannot guarantee optimality of nonconvex models [29, 30]. Thus, system designs determined by an optimizer coupled to TRNSYS are provided without any certificate of optimality. The authors of this article argue that rigorous guarantees of optimality are required for investment decision making.

Based on the modeling approach of Stuber [17], this article proposes new global dynamic optimization-based design models to perform rigorous technoeconomic analyses of several solar hybridization strategies. Specifically, we develop PV and electrical energy storage (EES) models. Therefore, this work establishes new models for assessing the economic feasibility of PVs with thermal storage or EES. As in [17], these models are specifically developed for deterministic global optimization approaches to ensure that the best-possible designs and project economics are determined for each technology and geographic location; necessary for new technology investment decision making. In addition to a comparative assessment of PTC and PV technologies with different storage approaches, we also explore the impacts of different natural gas rates on the economic feasibility of each technology.

This paper seeks to explore the economic feasibility of solar technology options to provide low- to medium-temperature IPH using rigorous deterministic global optimization. The developed models utilize hybridization with natural gas to reflect the current state of the IPH sector and its pursuit of decarbonization. In this paper, the open-source EAGO solver [31] is used to rigorously solve the proposed design problems to guaranteed global optimality. This paper is organized as follows: The main development of the models is provided in §2. Numerical experiments and their corresponding results and discussion are provided in §3. The paper is concluded in §4.

2. Model Development

This section presents the development of the mathematical models used for the optimal design and technoeconomic assessment of solar hybrid IPH systems. This includes the PV solar conversion model (§2.1), the overall solar hybrid IPH system model (§2.2), the economic models for each technology (§2.3), and the optimization model (§2.4).

2.1. Model for Photovoltaic Conversion of Irradiance to Electrical Power

In this section, a model is presented for the conversion of incident light into electrical power via the photovoltaic effect. The power output of a PV

panel is dependent on intrinsic properties of the panel that include the open circuit voltage V_{oc}, short circuit current I_{sc}, maximum power voltage V_{mp}, maximum power current I_{mp}, temperature coefficient for current α_T, and band gap parameters α, β, and E_{g0} [32]. These values are readily available from the manufacturer and are tabulated in Appendix C for the commercially available SunPower E19-320 module considered in this study. PV power output is also dependent on external factors, such as sunlight, incident angle, and temperature. NREL's National Solar Resource Database (NSRDB) [33] provides hourly typical meteorological year (TMY) data for temperature, direct normal irradiance (DNI) and diffuse horizontal irradiance (DHI). The incident angle of DNI is important, but not for DHI since the light is scattered. The incident light on PV panels is calculated based on the DNI, DHI, and incident angle of the DNI.

The PV model used in this paper follows the work of Sidibba et al. [32] and Mboumboue and Njomo [34]. The energy output of a PV solar panel can be modeled using Kirchhoff's Laws as illustrated in Figure 1. Kirchoff's

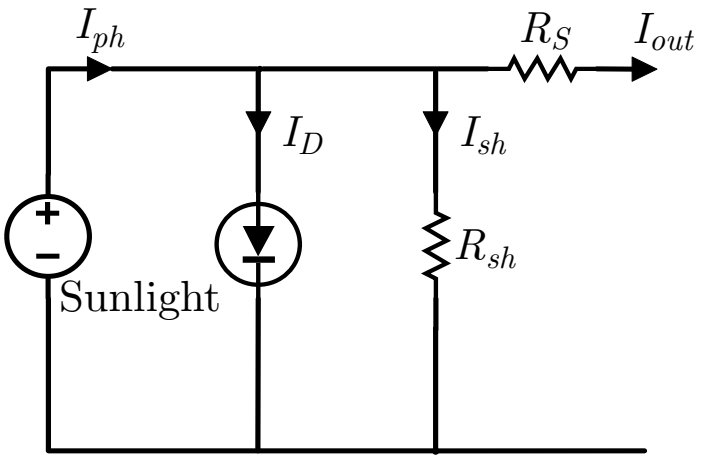

Figure 1: The circuit diagram of a solar cell shows that the light current, I_{ph} is lowered by the diode current I_D, the shunt current I_{sh}, and series resistance R_s. The PV model in this work is based on this representation.

Laws yield the following relationship:

$$I_{out} = I_{ph} - I_D - I_{sh}, \tag{1}$$

where light current I_{ph} represents the total electrical energy produced between the p-n junction and is reduced by the current flowing in reverse

through the diode I_D and shunt I_{sh}, and the series resistance R_s. The series resistance originates as the current moves through the solar cell and the metal contacts. The shunt current is caused by imperfections in the semiconductor material that cause some current to flow in reverse, reducing the usable current. This model assumes the shunt resistance is very large; thus $I_{sh} = 0$ [32].

The underlying equation for the power output P in watts is given by

$$P = \frac{nNk_BT_c}{q} \log\left(1 + \frac{I_{ph} - I}{I_0}\right) R_s I^2 \epsilon_r \epsilon_s \epsilon_i \epsilon_w. \tag{2}$$

Calculations to determine I_{ph}, I_0, R_s, and n can be found in Appendix D.1 and depend on the intrinsic properties of the PV cell and external factors. The power output is divided by the area of the panel, which is provided by the manufacturer and considered to be a design variable herein. Lastly, inefficiency parameters are incorporated to account for reflection ϵ_r, soiling ϵ_s, inverter ϵ_i, and wiring ϵ_w. These values are based on NREL's System Advisor Model [35] and can be found in Appendix C.

2.1.1. Tracking Systems

The DNI incident angle must be calculated at each moment in time to determine the corresponding incident light. The incident light E_e is given by

$$E_e = E_{e,\text{diff}} + E_{e,\text{dir}} \cos(\theta), \tag{3}$$

where $E_{e,\text{diff}}$ is the DHI, $E_{e,\text{dir}}$ is the DNI, and θ is the incident angle. The incident angle is the angle between the line perpendicular to the PV module and the incoming DNI, and it changes continuously. The angle changes in the east-west direction as the Earth rotates during a 24-hour period, and the angle changes in the north-south direction as the Earth revolves in a 365-day period. To absorb the maximum amount of sunlight, the PV module must minimize the incident angle. This can only truly be achieved using a control system that continuously adjusts the angle of the PV panel throughout the day/year in both the east-west and north-south directions using an automatic control system (i.e., two-axis tracking). Such systems are not considered in this study because of their relative cost and space limitations for large-scale industrial applications.

Conventional PV arrays that do not have automatic control systems are called *fixed* systems, or referred to as zero-axis tracking in this paper. To

minimize the incident angle of these arrays under the constraint that they cannot move, angled mount systems are used. For such mounts, the angle is set to the latitude of the installation with the PV array pointed towards the equator. The zero-axis tracking model used in this work is taken from Kalogirou [36] and can be found in Appendix D.3.

Alternatively, a single-axis (or one-axis) tracking PV array is able to further reduce the incident angle by utilizing a mounting system that fixes the array angle in one direction and an automatic control system adjusts the array angle in the other direction. The result is that these systems receive more sunlight than zero-axis tracking systems because they are able to further minimize the incident angle throughout the day or year, depending on the configuration. The one-axis tracking system considered in the proposed models faces east in the morning and west at night, and is fixed in the north-south direction. Due to moving parts and automatic control systems, one-axis tracking arrays cost more than zero-axis systems (see §2.3), but are less expensive and more suitable for larger-scale industrial applications than two-axis systems. The one-axis tracking model used in this study is based on the works of Stuber [17] and Kalogirou [36] and can be found in Appendix D.4.

2.2. Solar Hybrid Industrial Process Heat System

Our model of solar hybridization of IPH systems considers that the process demands can be met by three potential sources: solar collectors, stored energy, and natural gas. When multiple energy sources are available, the system must determine which source to prioritize. Solar collector energy is prioritized first, stored solar energy is second, and then natural gas is used as the last option. Using energy from the solar collector provides direct power to the process, circumventing any potential inefficiencies associated with energy storage. The objective of solar hybridization is to reduce natural gas combustion, yet practical implementations still rely on some natural gas combustion during overcast or nighttime operations.

There are two classes of solar hybridization that are considered in this work—PV and PTC. In total, this results in five possible solar module and storage configurations that will be studied: PV with zero-axis tracking and TES (PV0-TES) or EES (PV0-EES), PV with one-axis tracking and TES (PV1-TES) or EES (PV1-EES), and one-axis PTC with TES (PTC-TES). The model of Stuber [17] is used for PTC and TES, and so the focus of this

section is on the development of the class of PV systems models. Just as in [17], the models are developed based on the first law of thermodynamics.

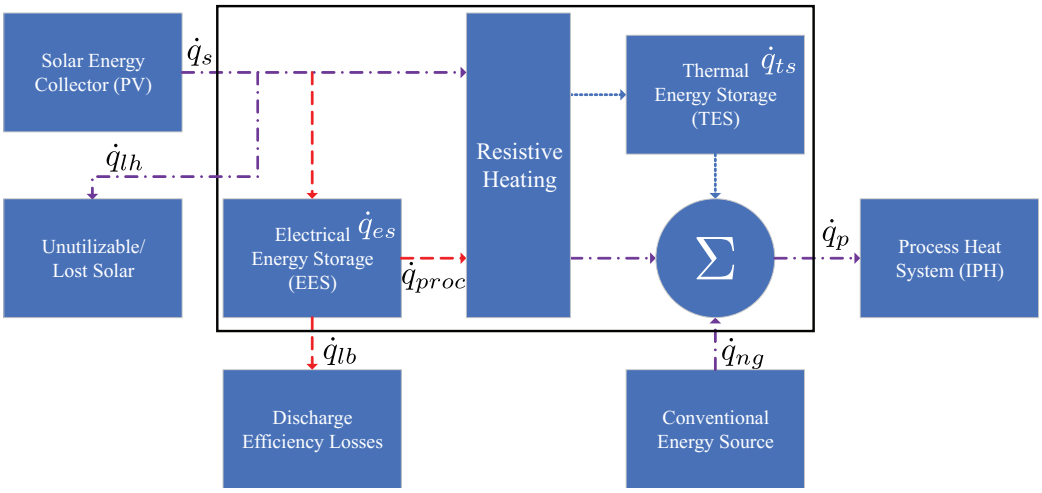

Figure 2: A block-flow diagram of the hybridized PV system is illustrated. Both electrical energy storage (EES) and thermal energy storage (TES) options are illustrated, but only one is considered at a time. Red dashed lines are used by EES system, blue dotted lines are used by TES system, and purple dotted/dashed lines are used by both systems. The solid black box indicates the boundary of the system for the energy balance. The energy storage terms $\dot{q}_{es}$ and $\dot{q}_{ts}$ are treated as accumulation terms in the relevant energy balance.

Figure 2 illustrates a block-flow diagram of the PV systems considered in this work. This diagram condenses the four new systems (not accounting for PTCs) into one figure with color-coded stylized arrows to denote which blocks and energy flow terms correspond to which system: purple dash-dot arrows apply to both TES and EES, blue dotted arrows apply only to TES, and red dashed arrows apply only to EES. The black box enclosing the energy storage/dispatching system represents the boundary of the system considered for the energy balance, i.e., the basis of load balancing control.

Modeling Assumptions. *The following simplifying assumptions are made to model the hybridized solar IPH system, which follow from Stuber [17]:*

1. *Heat losses to the environment from piping and heat exchangers (including resistive heaters) are negligible.*
2. *Heat losses to the environment from the PTC system are negligible.*

3. *Energy losses as a result of the degradation of the EES system over time are negligible.*
4. *The process system requires low to medium temperature IPH (i.e.,* $\leq$ 250°C*).*
5. *Heat is always available at or above the minimum temperature, as required by the IPH system.*
6. *The energy demand of the IPH system is not dependent on the state or design decisions of the solar energy system.*

Since the work of Stuber [17] only considered TES, the EES model is developed in this section. The boundary considered for the overall energy balance is centered around the energy dispatching system (black box in Figure 2). Energy inflows are from the solar energy collector (PV) and conventional energy (natural gas), and energy outflows are to the IPH system, unutilizable/lost solar energy, and battery discharge efficiency losses. Based on Figure 2, the hybridized IPH system with PV cells and lithium-ion EES is represented by the following dynamic energy balance:

$$\dot{q}_s + \dot{q}_{ng} = \dot{q}_p + \dot{q}_{es} + \dot{q}_{lh} + \dot{q}_{lb}, \tag{4}$$

where $\dot{q}_s$ is the electrical power provided by the solar system, $\dot{q}_{ng}$ is thermal power provided by the natural gas heating system, $\dot{q}_p$ is the thermal power demand of the industrial process, $\dot{q}_{es}$ is the instantaneous electrical power supply/demand of the lithium-ion batteries, $\dot{q}_{lh}$ is the lost solar power due to meeting the process demand and exceeding the maximum electrical energy storage capacity, and $\dot{q}_{lb}$ is the lost electrical power due to the round-trip efficiencies of lithium-ion batteries. The balance (4) implies that the energy flowing into the system is either from solar or natural gas, and the only way it can leave is to the process or to the environment in the form of excess or efficiency losses. Since the EES system charges and discharges with respect to time and is included within the boundaries of the energy balance, the storage term $\dot{q}_{es}$ can be thought of as an accumulation term. The convention chosen here is that if $\dot{q}_{es} < 0$, the storage system is discharging and $\dot{q}_{es} > 0$ if the storage system is charging.

It is important to note that in order to model PV configurations with TES, the overall energy balance of Stuber [17] is used with the $\dot{q}_s$ term reflecting the PV technology developed in §2.1. This is equivalent to (4) with the battery loss term $\dot{q}_{lb}$ being omitted and $\dot{q}_{es}$ replaced with $\dot{q}_{ts}$ to yield:

$$\dot{q}_s + \dot{q}_{ng} = \dot{q}_p + \dot{q}_{ts} + \dot{q}_{lh}. \tag{5}$$

The derivation and implications of the load balancing controls of PV-TES are considered analogous to PTC-TES in Stuber [17], and will therefore not be covered here. As such, the focus will stay on the EES dynamic energy balance (4).

As in [17], (4) is rearranged to focus on the storage device as the accumulation term to get the following differential equation:

$$\frac{dq_{es}}{dt} = \dot{q}_s - \dot{q}_p - \dot{q}_a - \dot{q}_{lb},\ t \in [0, t^{\text{end}}], \tag{6}$$

where the ancillary power term $\dot{q}_a = \dot{q}_{lh} - \dot{q}_{ng}$ was introduced for convenience to account for the energy input from natural gas and the unutilizable solar energy lost.

Using a discrete time stepsize of $h = \Delta t$ (1 h for standard solar resource data) and applying the explicit Euler integration scheme to (6) yields:

$$q_{es}^{i+1} = q_{es}^{i} + h(\dot{q}_s^i - \dot{q}_p^i - \dot{q}_a^i - \dot{q}_{lb}^i),\ q_{es}^1 = 0. \tag{7}$$

Since the EES has a finite capacity, we can write:

$$q_{es}^{i+1} = \text{mid}\{\dot{q}_p^{peak} x_{es}, 0, q_{es}^i + h(\dot{q}_s^i - \dot{q}_p^i - \dot{q}_{lb}^i)\}, \tag{8}$$

where x_{es} is the storage capacity of the batteries (in h), and $\dot{q}_p^{peak}$ is the maximum IPH demand. The $\text{mid}(\cdot, \cdot, \cdot)$ selects the middle value of its three arguments to capture the finite capacity of the battery, which ensures that the storage level never exceeds its maximum capacity or its minimum of zero.

Combining (7) and (8) yields the overall energy balance:

$$\begin{aligned} h\dot{q}_a^i &= q_{es}^i + h(\dot{q}_s^i - \dot{q}_p^i - q_{lb}^i) - q_{es}^{i+1} \\ &= q_{es}^i + h(\dot{q}_s^i - \dot{q}_p^i - q_{lb}^i) - \text{mid}\{\dot{q}_p^{peak} x_{es}, 0, q_{es}^i + h(\dot{q}_s^i - \dot{q}_p^i - \dot{q}_{lb}^i)\}. \end{aligned} \tag{9}$$

Specifically, (9) represents the difference between the total amount of energy that must be stored/discharged at time i (i.e., $\dot{q}_{es}^i + h(\dot{q}_s^i - \dot{q}_p^i)$) and the amount of energy stored in the battery at time $i+1$ (i.e., $\text{mid}\{\dot{q}_p^{peak}, 0, \dot{q}_{es}^i + h(\dot{q}_s^i - \dot{q}_p^i - \dot{q}_{lb}^i)\}$). As such, it provides information on the source of energy supplied to the system at every time step i.

When considering an imperfect energy storage system, there are several terms that impact performance and load balance accounting. The storage

model dynamics (both TES and EES) are based on the first law of thermodynamics, and do not consider other complications such as battery degradation over time, or charging conditions/behavior near the maximum and minimum capacities. This establishes a best-case scenario in terms of solar energy usage, which is an adequate basis to determine technoeconomic feasibility. Generally speaking, the amount discharged $\dot{q}_d$ must be greater than the amount sent to the IPH system $\dot{q}_{proc}$, with the excess being lost $\dot{q}_{lb}$ due to inefficiencies. This is accounted for in this model with the energy balance

$$\dot{q}_d^i = \dot{q}_{proc}^i + \dot{q}_{lb}^i. \tag{10}$$

This balance assumes the case of $\dot{q}_s^i < \dot{q}_p^i$ and $q_{es}^i > |h(\dot{q}_s^i - \dot{q}_p^i)|$ where we have $\dot{q}_{proc}^i = \dot{q}_p^i - \dot{q}_s^i$. First, assume that q_{es}^i is greater than $h\dot{q}_{proc}^i$ by a factor of $1/\eta$, where η represents the round-trip efficiency of the battery. In this work, the definition of *conversion round-trip efficiency* (i.e., the ratio of energy discharged per unit of energy charged) provided by Schimpe et al. [37] is used for the round-trip efficiency η. We can then define:

$$\dot{q}_d^i = \frac{\dot{q}_{proc}^i}{\eta}. \tag{11}$$

In this case, the losses are naturally expressed as the difference between the energy that is discharged from the system and the energy that is actually delivered to the IPH process:

$$\dot{q}_{lb}^i = \dot{q}_d^i - \dot{q}_{proc}^i = \left(\frac{1-\eta}{\eta}\right)\dot{q}_{proc}^i. \tag{12}$$

Next, consider the other case where $\dot{q}_{es}^i$ is not greater than $\dot{q}_{proc}^i$ by a factor of $1/\eta$. Then, we simply calculate the losses based on the remaining capacity of the battery being discharged: $\dot{q}_{lb}^i = (1-\eta)\dot{q}_{es}^i$. Combining these two cases gives us the following expression for EES discharging losses:

$$h\dot{q}_{lb}^i = \left(\frac{1-\eta}{\eta}\right)\text{mid}\{\eta q_{es}^i, 0, h(\dot{q}_p^i - \dot{q}_s^i)\}. \tag{13}$$

This understanding of the EES model aids in providing insight into the load balancing ancillary power term $\dot{q}_a$. All implications on the value of $\dot{q}_a$ are as follows:

1. $(\dot{q}_s^i > \dot{q}_p^i) \wedge (q_p^{peak} x_{es} - q_{es}^i < h(\dot{q}_s^i - \dot{q}_p^i)) \iff \dot{q}_a^i > 0$
   Solar power exceeds the IPH demand for this time step and the available battery capacity is too small to store the full amount of excess energy,meaning that some energy will be lost due to reaching the maximum storage capacity. Therefore, $\dot{q}_{lb}^i = 0 \wedge \dot{q}_{ng}^i = 0 \wedge \dot{q}_{lh}^i = \dot{q}_a^i$.
2. $(\dot{q}_s^i < \dot{q}_p^i) \wedge (\eta q_{es}^i < |h(\dot{q}_s^i - \dot{q}_p^i)|) \Rightarrow \dot{q}_a^i < 0$.
   Instantaneous solar power is insufficient to meet the IPH demand, so the EES will go into a discharging state until the remaining capacity is drained. At this point, natural gas will be used. Therefore, $\dot{q}_{lb}^i = (1-\eta)\dot{q}_{es}^i \wedge \dot{q}_{ng}^i = -\dot{q}_a^i \wedge \dot{q}_{lh}^i = 0$.
3. $(\dot{q}_s^i < \dot{q}_p^i) \wedge (\eta q_{es}^i > |h(\dot{q}_s^i - \dot{q}_p^i)|) \Rightarrow \dot{q}_a^i = 0$
   Instantaneous solar power does not meet the IPH demand, but the difference between supply and demand is less than the available stored energy. Therefore, $\dot{q}_{lb} = (1-\eta)\dot{q}_{es} \wedge \dot{q}_{ng} = 0 \wedge \dot{q}_{lh} = 0$
4. $(\dot{q}_s^i = \dot{q}_p^i) \vee \big((\dot{q}_s^i > \dot{q}_p^i) \wedge (\dot{q}_p^{peak} x_{es} - q_{es}^i \geq h(\dot{q}_s^i - \dot{q}_p^i))\big) \Rightarrow \dot{q}_a^i = 0$
   If the solar energy supply and the IPH demand are exactly equal, there would be no losses and no need for natural gas or energy storage. If instantaneous solar exceeds the IPH demand and there is enough available capacity in the battery, the excess will be stored. In both cases, $\dot{q}_{lb} = \dot{q}_{ng} = \dot{q}_{lh} = 0$.

Lastly, the performance of the PV-EES system is assessed by the solar fraction:

$$SF = \frac{\sum_i h(\dot{q}_s^i - \dot{q}_{lh}^i - \dot{q}_{lb}^i)}{\sum_i h\dot{q}_p^i} = 1 - \frac{\sum_i h\dot{q}_{ng}^i}{\sum_i h\dot{q}_p^i}, \tag{14}$$

where we note that the definition provided in [17] does not account for the $\dot{q}_{lb}^i$ term since EES was not considered in that work. For systems with TES, (14) will be used with $\dot{q}_{lb}^i$ omitted, as in [17].

To demonstrate the behavior of the developed PV and EES models versus the PTC-TES model of [17] and to illustrate the dynamic energy dispatching, realistic energy profiles are shown in Figure 3 for a three-day period with an overlay of the incident light profile (black curve) for the same period. The profile starts at midnight, and the system is initially powered by energy stored (red bars) from the previous day. Due to the round-trip efficiency η that results in losses when discharging, the EES is not able to provide energy for as many hours as the TES, despite having the same charged capacity. The first day has clear skies, and the process is almost entirely powered by the solar system. The second day is cloudy, and as a result, there is less surplus

energy generated to charge the storage system. As such, more natural gas is used (gray-blue bars). On these cloudy days, PVs capture and convert more light than PTCs because PTCs cannot use diffuse light.

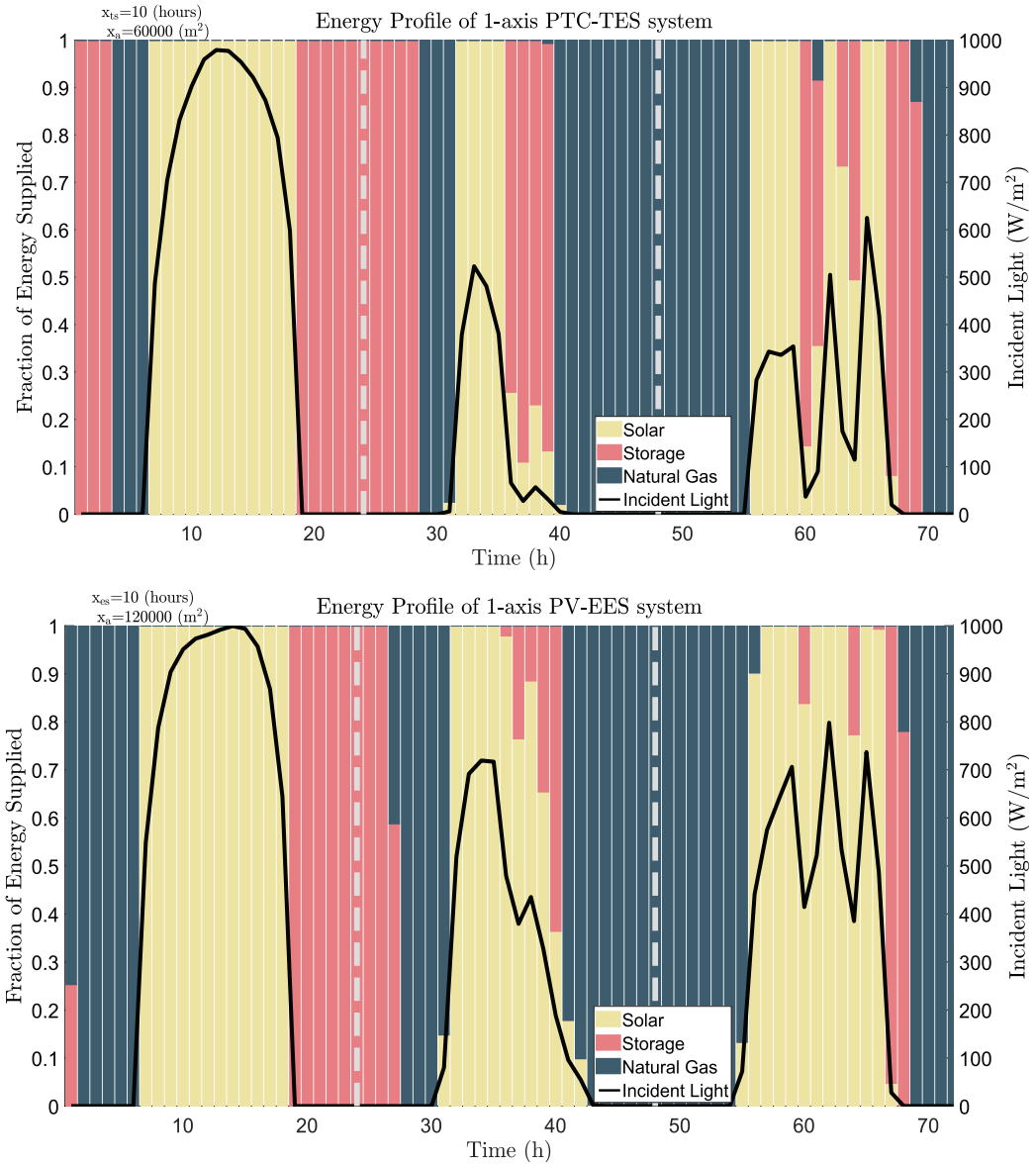

Figure 3: The energy profiles supplied by a PTC-TES (top) and a PV1-EES (bottom) system across a three-day period compared to the incident light. Note that the PTC system has a lower aperture area than the PV system, however, they provide roughly the same power output. The plots start at midnight, and each day is separated by vertical dashed gray lines. The system starts using stored energy from the previous day. Early in the morning, the storage is depleted and the system switches to natural gas. The first day is very sunny and leads to a high solar fraction. The second and third days are partially cloudy and rely heavily on natural gas.

2.3. Economic Models

The relevant economic metrics to consider when assessing the feasibility of hybridization strategies involve accurate capital cost models for each type of energy technology: natural gas, PTC, PV with 0-axis tracking, PV with 1-axis tracking, TES, and EES. The PTC and TES cost models used herein are provided in [17]. They utilize economies of scale using standard power-law relationships, to account for discounted pricing at bulk quantities. The cost models of the remaining technologies in this study are regressions of aggregate data from technical reports published by the National Renewable Energy Laboratory (NREL) [38, 39, 40, 41, 42]. NREL developed these reports and datasets based on literature review, the System Advisor Model (SAM), and manufacturer quotes. NREL PV data was taken from Wood Mackenzie and the Solar Energy Industries Association (SEIA), which uses over 200 utilities, state agencies, installers, and manufacturers [38]. From these data, pre-exponential factors and scaling exponents are developed for each technology. With the original capital cost model modified for the five different permutations of technologies, five discount pricing models emerge:

$$C_{cap,0}^{PTC}(x_{ts}, x_a) = 425 x_a^{0.92} + 45.14(\dot{q}_p^{peak} x_{ts})^{0.91}, \tag{15}$$

$$C_{cap,0}^{PV0T}(x_{ts}, x_a) = 200.18 x_a^{0.9617} + 45.14(\dot{q}_p^{peak} x_{ts})^{0.91}, \tag{16}$$

$$C_{cap,0}^{PV0E}(x_{es}, x_a) = 200.18 x_a^{0.9617} + 736.38 \left(\dot{q}_p^{peak} \frac{x_{es}}{\psi} \right)^{0.9355}, \tag{17}$$

$$C_{cap,0}^{PV1T}(x_{ts}, x_a) = 223.49 x_a^{0.9586} + 45.14(\dot{q}_p^{peak} x_{ts})^{0.91}, \tag{18}$$

$$C_{cap,0}^{PV1E}(x_{es}, x_a) = 223.49 x_a^{0.9586} + 736.38 \left(\dot{q}_p^{peak} \frac{x_{es}}{\psi} \right)^{0.9355}, \tag{19}$$

where the superscripts PTC, $PV0T$, $PV0E$, $PV1T$, and $PV1E$ correspond to the technology configurations PTC-TES, PV0-TES, PV0-EES, PV1-TES, and PV1-EES, respectively.

The design variables are defined as $\mathbf{x} = (x_{ts}, x_a)$ or $\mathbf{x} = (x_{es}, x_a)$ depending on the technology considered. They represent the size of the energy storage system in hours (i.e., x_{ts} for TES and x_{es} for EES) and the aperture area of the solar array x_a in m^2. To simulate the technical performance of the EES, x_{es} represents the *usable* battery capacity. Conventionally, the battery is never 100% charged or completely depleted, so a factor $\psi \in (0, 1]$ is introduced that represents the depth of discharge (DoD). This factor effectively

scales up the actual battery design (since x_{es} is divided by ψ) to account for the desired operating capacity. For example, the battery is considered to operate between 10%-90% of its total capacity, and therefore the DoD is set to $\psi = 0.8$. Within this window, the open circuit potential of the battery and the round-trip efficiency are relatively constant [37]. Thus a constant η value in the model is accurate and the resistive heating element is always expected to satisfy the required temperature condition (Assumption 5) without conversion losses (Assumption 1). The units of the outputs of these equations are US$.

2.4. Optimal Design and Technoeconomic Assessment

The technical and economic models developed in this work are formulated as functions of the design variables $\mathbf{x}$ specifically to enable the use of formal mathematical optimization in the design of hybridization strategies. This ensures that only guaranteed optimal designs are evaluated for economic feasibility.

The objective function for the optimal design problem is formulated as the lifecycle cost savings (LCS):

$$f^k_{LCS}(\mathbf{x}) = \sum_{i=1}^{t_{\text{life}}} \frac{SF(\mathbf{x})C_{p,i} - C^k_{cap,i}(\mathbf{x}) - C_{om,i}(\mathbf{x})}{(1+r)^i}, \tag{20}$$

where t_{life} is the project lifetime (in years), r is the capital discount rate, $C_{p,i}$ is the cost of natural gas at year i, $C^k_{cap,i}$ is the annualized cost of capital (including debt service) in year i for technology k, and $C^k_{om,i}$ is the annual operating and maintenance cost of technology $k \in \{PTC, PV0T, PV0E, PV1T, PV1E\}$ at year i. The expression SF was originally defined in (14) and is expressed here as a function of the relevant design variables $\mathbf{x}$ as

$$SF(\mathbf{x}) = \frac{\sum_i h(\dot{q}^i_s(\mathbf{x}) - \dot{q}^i_{lh}(\mathbf{x}) - \dot{q}^i_{lb}(\mathbf{x}))}{\sum_i h\dot{q}^i_p} = 1 - \frac{\sum_i h\dot{q}^i_{ng}(\mathbf{x})}{\sum_i h\dot{q}^i_p},$$

with $\dot{q}^i_{lb} = 0$, for all i, for thermal storage systems. Note that in this formulation, the relationships (9) and (13) are embedded in the definition of $SF(\cdot)$. Furthermore, the smooth approximation of the $\text{mid}(\cdot,\cdot,\cdot)$ operator formulated in [17] is used for (9) and (13) to ensure differentiability of the model.

In some applications, it may be useful to specify a minimum solar fraction $\xi \geq 0$. Therefore, the following inequality constraint is formulated for the optimization problem:

$$g(\mathbf{x}, \xi) = \xi - SF(\mathbf{x}) \leq 0, \tag{21}$$

with $\xi \in [0, 1]$, and $\xi = 0$ represents the unconstrained case since $SF(\cdot) \geq 0$ by definition. The optimal design problem is then formulated as:

$$\begin{aligned} f^*_{LCS} = &\max_{\mathbf{x} \in X} f^k_{LCS}(\mathbf{x}) \\ &\text{s.t. } g(\mathbf{x}, \epsilon) \leq 0 \\ &\quad X = \{\mathbf{x} \in \mathbb{R}^2_+ : \mathbf{x}^L \leq \mathbf{x} \leq \mathbf{x}^U\}. \end{aligned} \tag{22}$$

This optimization formulation will be used in the next section to study the technoeconomic feasibility of solar IPH hybridization strategies.

3. Numerical Experiments and Results

The models developed in this paper allow for the determination of economically optimal solar system sizes for industrial heating processes hybridized with natural gas. In this section, we will analyze the following case studies: unconstrained systems designs §3.1, constrained systems designs §3.2, a survey of process demand scales §3.3, higher natural gas prices §3.4, and the future trends of the electrified technologies §3.5. The cost parameters for these technologies can be found in Appendix E, and the capital cost models can be found in (15)-(19).

All models presented here were implemented in the Julia programming language [43] v1.7.0. The hourly solar radiation data were taken from the TMY data obtained from NREL's NSRDB [33]. Operating and maintenance costs were omitted from each study to better compare the capital costs of solar to natural gas costs. Each optimization problem is solved to guaranteed global optimality using the EAGO.jl solver [31] v0.6.1 with the appropriate convex envelopes developed by Stuber [17, Thm. 3]. IPOPT [20] was used to solve the local and convex optimization subproblems via Ipopt.jl v0.6.5. JuMP [44] v0.21.5 was used to model the optimization problems. For each problem solved, the solver outputs the optimal solar system size $\mathbf{x}^*$, the corresponding optimal solution value f^*_{LCS}, and the optimal solar fraction value

SF^*. For each case, a constant DoD of $\psi = 0.8$ is used, as is a constant and conservative round-trip efficiency $\eta = 0.85$, based on the validated work of Schimpe et al. [37]. All technologies in this study are subject to a constant demand profile over a 30-year lifecycle of the system. Figure 4 and Figure 5 are presented to illustrate the objective function and solar fraction surfaces over the design/decision space for each technology consideration for a base-case scenario. Deterministic global optimization identifies a design that results in the highest LCS (as analyzed in the subsequent case studies). A solar fraction constraint, as formulated in (22), restricts the feasible set to the corresponding ξ-superlevel set, which is explored in §3.2.

3.1. Unconstrained Case Study

This case study examines the feasibility of unconstrained ($\xi = 0$) solar systems located in three locations across the continental US: Firebaugh, CA; Aurora, CO; and Weston, MA; with a process demand of 10 MW and using a national average price of commercial natural gas of US$9.52 per MMBTU as of July 2021, listed in Appendix E.

Regarding economic feasibility, PTCs outperform PVs, and TES outperform EES. In the left columns of Figure 4 and Figure 5, the aperture area and storage size are plotted against the LCS value f^k_{LCS} for each technology in Firebaugh, CA. Although they are more expensive per unit area, PTCs have a higher LCS because they have a significantly higher conversion efficiency of incident light compared to PVs. On average, PTCs convert 63.9% of incident light into energy, while PVs only convert 17.1%. TES outperforms EES because the capital cost is significantly lower. In Figure 5, the EES plots illustrate greater sensitivities to storage size than aperture area due to the high EES capital cost prefactor (listed in Appendix E). Furthermore, TES can use all its storage capacity, while EES can only be charged between 10% and 90% due to the DoD. To compare their ability to meet process demands, the solar fractions of each technology are compared.

PTCs with TES have higher SF values as compared to their PV and EES counterparts. The SF value represents the fraction of the total process demand that is supplied by solar technologies via solar modules and energy storage. As seen in the right columns of Figure 4 and Figure 5, PTC systems have greater sensitivities with respect to aperture area as compared to PVs. This means that a PTC system can reach the demands of the process with much lower aperture areas compared to a PV system. This is explained by the higher conversion of incident light to usable energy by PTCs compared

Table 1: The optimal solar system sizes, corresponding lifecycle cost savings f^*_{LCS}, and solar fractions are tabulated for the case study of §3.1. These results were obtained for an unconstrained 10MW process with natural gas priced at $9.52 per MMBTU. PTC-TES systems have the highest f^*_{LCS}, at least four times higher than the best PV system (PV1-TES) in all locations.

Location	System	x^*_a (10^4 m^2)	x^*_{ts}/x^*_{es} (h)	f^*_{LCS} (10^6 US$)	SF^* (%)
Firebaugh, CA	PTC-TES	4.94	13.0	12.4	73.6
	PV1-TES	12.3	10.6	3.17	64.3
	PV0-TES	18.6	13.6	1.45	78.2
	PV1-EES	6.07	0	1.99	31.7
	PV0-EES	5.84	0	0.671	24.6
Aurora, CO	PTC-TES	6.10	16.0	11.9	78.7
	PV1-TES	13.0	10.9	1.90	62.6
	PV0-TES	18.2	13.7	1.05	75.6
	PV1-EES	6.01	0	1.34	29.2
	PV0-EES	5.68	0	0.546	23.5
Weston, MA	PTC-TES	6.50	17.9	7.24	65.3
	PV1-TES	0	0	0	0
	PV0-TES	0	0	0	0
	PV1-EES	0	0	0	0
	PV0-EES	0	0	0	0

to PVs. PV1-TES reaches a higher maximum SF value than PV1-EES due to EES accounting for the DoD and the discharge losses, which enforces the availability of only a fraction of the designed battery capacity, while TES has no such limitations on the availability of its design capacity.

The location of the system significantly impacts the feasibility of solar hybridization. As seen in Table 1, every optimal system in Firebaugh, CA and Aurora, CO has a nonzero aperture area. However, in Weston, MA, all PV technologies considered are economically infeasible due to the lower solar resource and higher average incident angle. The higher collection efficiency of PTCs allows PTC-TES hybridization to be economically feasible, even in Weston, MA.

3.2. Constrained Case Study

In addition to a pure technoeconomic analysis for optimal solar system design, environmental considerations may also be taken into account. This

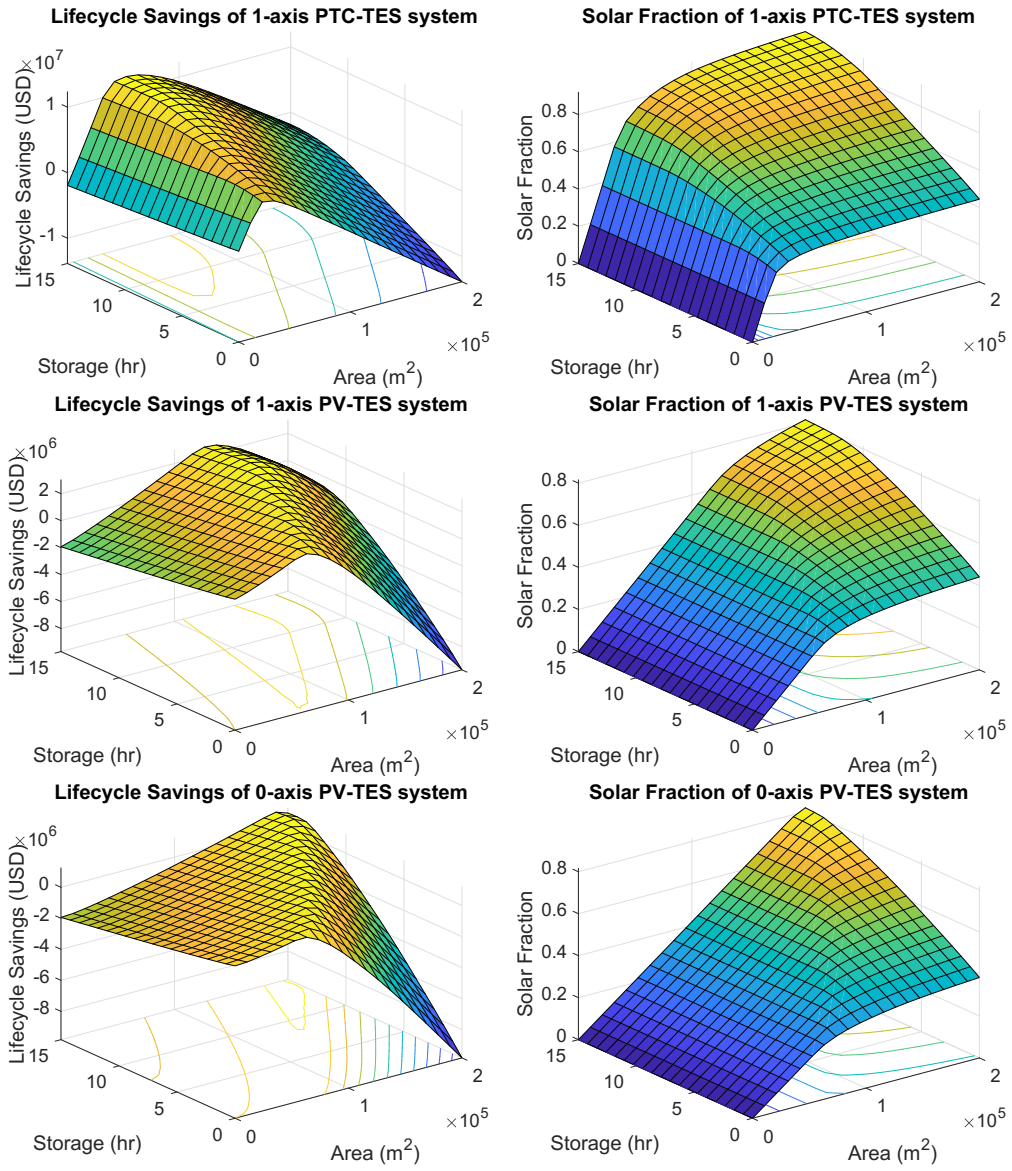

Figure 4: The lifecycle cost savings (LCS) and solar fraction (SF) are plotted for systems using PTC, PV1 and PV0 for energy collection and thermal energy storage (TES). These results were obtained for a 10MW process in Firebaugh CA with natural gas priced at \$9.52 per MMBTU. The LCS graphs illustrate the nonconvexity of the objective functions and highlight the need for rigorous global optimization.

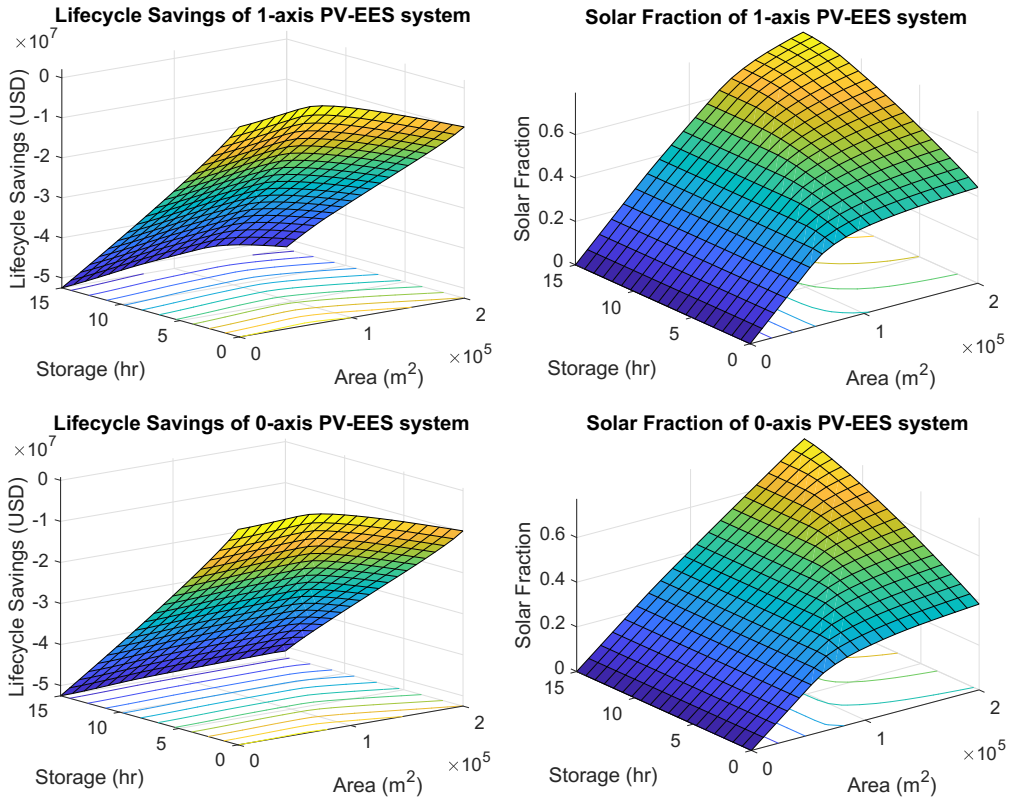

Figure 5: The lifecycle cost savings (LCS) and solar fractions (SF) are plotted for systems using PV1 and PV0 for energy collection and electrical energy storage (EES). These results were obtained for the base-case study of a 10MW process in Firebaugh, CA with natural gas priced at \$9.52 per MMBTU. EES systems have a very different shape and lower optimal LCS value than the TES systems found in Figure 4 due to their higher cost.

may be achieved by adding the solar fraction constraint (21) and introducing the parameter ξ that represents the lower bound on the solar fraction for an optimal design. This ensures that a greater share of renewable energy is used and, in turn, reduces natural gas combustion. However, this also results in an economic performance that cannot be better than the unconstrained case of §3.1. This can be seen in Figure 4 and Figure 5 where greater SF values (right columns) correspond with lower f^k_{LCS} values (left columns). Aside from the introduction of the SF constraint, all other conditions are the same as in §3.1.

The results of the constrained optimal design problems are presented in Table 2. As expected, SF-constrained systems have lower f^*_{LCS} values compared to unconstrained systems. The design trends also differ from Table 1. In Firebaugh and Aurora, The f^*_{LCS} of the PV0-TES case is positive, while the f^*_{LCS} of the PV1-TES case is very negative. This difference between the constrained and unconstrained cases is attributed to the topology of the f^k_{LCS} functions shown in Figure 4. The surfaces of both f^{PV0T}_{LCS} and f^{PV1T}_{LCS} are similar in shape; however, f^{PV0T}_{LCS} is flatter in the vicinity of the optimal solution, allowing for reduced LCS losses when deviating from the maximum. This flatter shape is due to the lower capital cost of PV0-TES compared to PV1-TES. In the LCS graph of PV1-EES, any system storage size greater than zero results in negative savings, which implies that more money is saved by losing excess energy than buying lithium-ion batteries to store it for later.

Since the optimal SF values of §3.1 are all below 85%, setting $\xi = 0.85$ in this case study forces the optimal designs to have larger apertures x^*_a and greater storage capacities x^*_{ts}/x^*_{es}. When comparing the optimal designs of the constrained case with the unconstrained case of §3.1, the optimal designs are indeed much larger in both apertures and storage capacities. In all TES cases, storage capacities increase disproportionately to aperture areas, which means that for high SF values, it is more economical to reduce solar losses $\dot{q}_{lh}$ as additional TES becomes cheaper than additional aperture area. However, for PV-EES cases in each location, larger solar apertures are favored compared to PV-TES as a result of EES being significantly more expensive than TES. For example, for Weston, PV1-EES has 44.8% more solar aperture area than PV1-TES (41.7×10^4 m^2 versus 28.8×10^4 m^2) but 54% less storage capacity (15 h versus 32.6 h). Similar trends are apparent for Firebaugh and Aurora. This is consistent with the economic trends discussed above that it is economically advantageous to lose excess energy (as $\dot{q}_{lh}$) than to invest in EES at its current price.

Table 2: The optimal solar system sizes, corresponding lifecycle cost savings f^*_{LCS}, and solar fractions are tabulated for the case study of §3.2. Constraining the solar fraction to be at least 85% forces the solar system designs to become large, and sometimes even negative investments. These results were obtained for a 10MW process with natural gas priced at \$9.52 per MMBTU.

Location	System	x^*_a (10^4 m^2)	x^*_{ts}/x^*_{es} (h)	f^*_{LCS} (10^6 US\$)	SF^* (%)
Firebaugh, CA	PTC-TES	7.45	21.7	11.3	85.0
	PV1-TES	21.5	22.8	-2.25	85.0
	PV0-TES	21.3	20.5	0.087	85.0
	PV1-EES	28.5	13.3	-53.9	85.0
	PV0-EES	26.7	14.9	-55.0	85.0
Aurora, CO	PTC-TES	7.31	21.1	11.5	85.0
	PV1-TES	21.4	22.9	-2.11	85.0
	PV0-TES	21.0	18.5	0.45	85.0
	PV1-EES	28.0	13.6	-54.1	85.0
	PV0-EES	27.0	14.6	-54.5	85.0
Weston, MA	PTC-TES	10.6	38.0	5.37	85.0
	PV1-TES	28.8	32.6	-11.2	85.0
	PV0-TES	26.6	31.6	-6.65	85.0
	PV1-EES	41.7	15.0	-73.2	85.0
	PV0-EES	41.2	15.7	-72.0	85.0

3.3. Process Demand Dependence

In this section, the effects of the process demand are examined for IPH demands of 0.1 MW, 1 MW, and 10 MW under the same unconstrained conditions as §3.1. The normalized optimal design results are presented in Figure 6 and the economics are tabulated in Table 3 (see Table A.1 for the complete solution results).

Regardless of the process demand, PTCs outperform PVs and TES outperform EES. This analysis is influenced by two parts: the economies of scale for these technologies and their effectiveness/efficiency in utilizing solar energy. Only examining the economies of scale would lead to the prediction that the difference between PV and PTC arrays would be comparatively smaller for small systems and comparatively larger for large systems. This is because the capital cost models for PV system configurations introduced in §2.3 have greater exponent values on x_a and x_{ts}/x_{es} than the PTC models. However, the analysis of technologies is more complicated. While the smaller

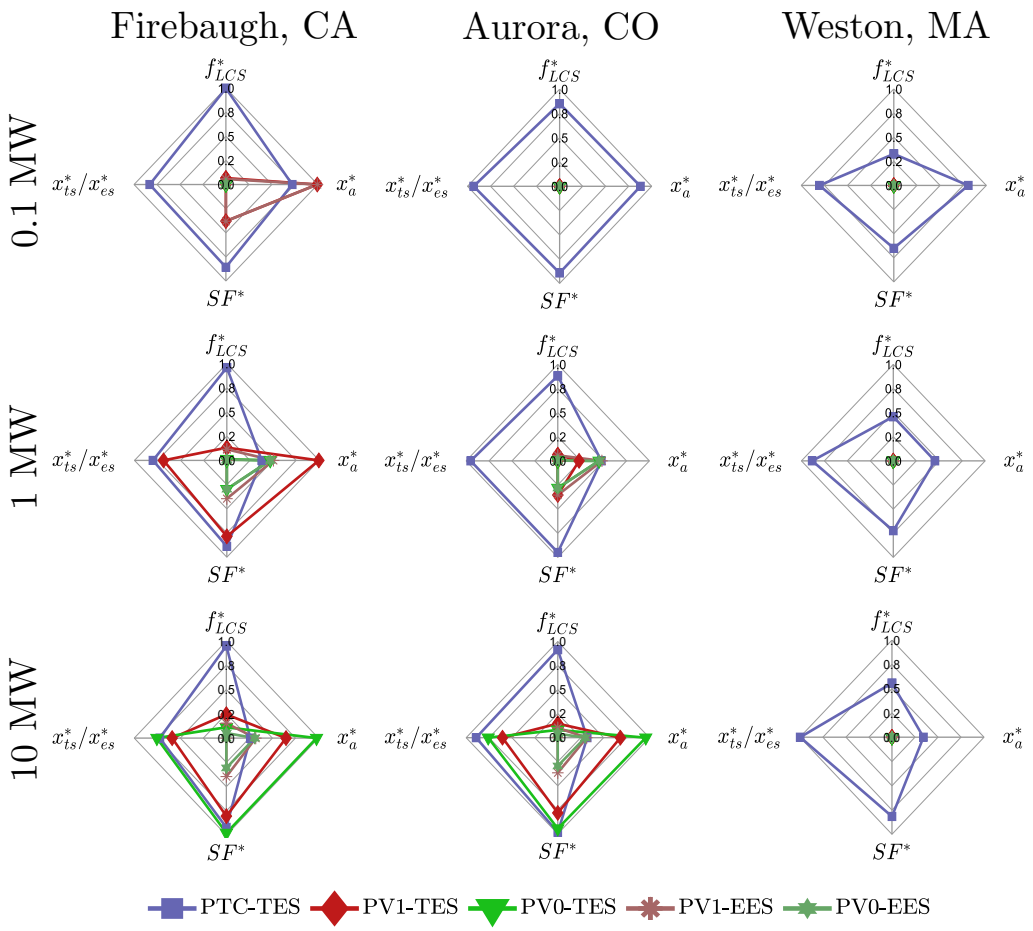

Figure 6: The results of the case study in §3.3 are plotted. For natural gas priced at \$9.52/MMBTU, radar plots illustrate the normalized optimal lifecycle cost savings (f^*_{LCS}), aperture area (x^*_a), solar fraction (SF), and thermal energy storage (x^*_{ts}) or electrical energy storage (x^*_{es}) for PTC-TES, PV1-TES, PV0-TES, PV1-EES, PV0-EES systems in three locations and across three process demands. The values were normalized for each process demand using the highest optimal value (rounded up to two significant figures) for each variable. Tabulated results can be found in Table A.1.

size would favor the cost of PVs over PTCs, there are several other factors that impact the f^*_{LCS} value that also vary with size. Such factors include their degree of hybridization with natural gas, and the ability to charge the energy storage device even with small aperture areas. Thus, rigorous optimization, as conducted herein, is necessary for a complete technoeconomic assessment.

The numerical results of the model predict that the difference between PVs and PTCs is actually comparatively larger in the small demand systems. PTC systems have optimal LCS values 15 times higher than the best PV system at 0.1 MW and have LCS values only 4 times higher than the best PV system at 10 MW. In the case of energy storage, the capital cost of EES is too high compared to that of TES, and thus it is not favorable for IPH applications, regardless of the process demand. The vast differences in optimal LCS across different process demands can be elucidated by exploring their corresponding optimal system sizes.

The process demands and locations dramatically affect the optimal system sizes, as seen in Figure 6. For the 10 MW systems, the optimal PTC system in Weston has a larger TES capacity than the optimal PTC system in Firebaugh or Aurora. This is because Weston has lower irradiance and needs more storage capacity to reduce natural gas consumption and maximize the LCS. In some cases, the optimal PV system has no storage with a nonzero aperture area. This is because the aperture area is too small or the irradiance is too little to generate a sufficient energy surplus that can be stored. Figure 6 also highlights how small the optimal system sizes become for PV systems paired with 0.1 MW and 1 MW IPH systems compared to PTC systems, especially in locations with reduced insolation. As expected, examining the optimal designs shows that the higher costs of PVs results in less hybridization and, in turn, greater natural gas consumption and lower f^*_{LCS} values compared to PTC designs. To explore this further, we consider a scenario with higher gas prices in the next section.

Table 3: The optimal lifecycle cost savings f^*_{LCS} are tabulated for the considered technologies at three process demand sizes for the case study in §3.3. These results were obtained for natural gas priced at \$9.52 per MMBTU. PTC systems perform significantly better compared to PV systems, especially for smaller IPH demand.

Location	System	0.1 MW	1 MW	10 MW
Firebaugh, CA	PTC-TES	84,800	1,060,000	12,400,000
	PV1-TES	5,680	145,000	3,170,000
	PV0-TES	0	14,100	1,450,000
	PV1-EES	4,880	126,000	1,990,000
	PV0-EES	0	7,710	671,000
Aurora, CO	PTC-TES	72,400	969,000	11,900,000
	PV1-TES	0	69,000	1,900,000
	PV0-TES	0	3,490	1,050,000
	PV1-EES	0	62,600	1,340,000
	PV0-EES	0	0	546,000
Weston, MA	PTC-TES	27,700	504,000	7,240,000
	PV1-TES	0	0	0
	PV0-TES	0	0	0
	PV1-EES	0	0	0
	PV0-EES	0	0	0

3.4. High Natural Gas Prices

In this case study, the same process scales as the previous section are considered; however, the natural gas price is doubled to a value of US\$19.04 per MMBTU. This could represent cases of carbon emissions penalties and/or reductions in gas production/availability.

The normalized optimal design results of this study are presented in Figure 7 with the economics tabulated in Table 4 (see Table B.1 for the complete solution results). Not only are the optimal solar system sizes larger than those corresponding to the lower natural gas price, but the gap between PTCs and PVs has been greatly reduced. Additionally, the optimal system sizes do not significantly change across location or process size as seen in Figure 7. PTCs still outperform PVs economically in all locations and IPH demand scales, but the gap is reduced for higher natural gas prices versus the lower natural gas prices. Figure 7 shows that PV-TES systems are competitive with PTC systems even for small process demands and locations with reduced sunlight.

At normal gas prices, PTCs have an f^*_{LCS} value that is larger than the best PV option (PV1-TES) by a factor of 15 and a factor of 4 for the 0.1

Table 4: The optimal lifecycle cost savings f^*_{LCS} are tabulated for the considered technologies at three process demand sizes for the case study in §3.4. These results were obtained for natural gas priced at $19.04 per MMBTU. PTCs are favored economically over PV at all scales.

Location	System	0.1 MW	1 MW	10 MW
Firebaugh, CA	PTC-TES	302,000	3,330,000	36,200,000
	PV1-TES	192,000	2,150,000	23,700,000
	PV0-TES	200,000	2,260,000	25,000,000
	PV1-EES	102,000	1,110,000	12,000,000
	PV0-EES	70,300	785,000	8,620,000
Aurora, CO	PTC-TES	303,000	3,370,000	37,000,000
	PV1-TES	181,000	2,080,000	23,300,000
	PV0-TES	198,000	2,270,000	25,400,000
	PV1-EES	89,100	992,000	10,900,000
	PV0-EES	66,400	746,000	8,250,000
Weston, MA	PTC-TES	221,000	2,630,000	30,200,000
	PV1-TES	110,000	1,380 000	16,600,000
	PV0-TES	122,000	1,530,000	18,400,000
	PV1-EES	57,000	672,000	7,690,000
	PV0-EES	42,300	507,000	5,860,000

MW and 10 MW IPH scales, respectively. With doubled natural gas prices, PTCs have an f^*_{LCS} value that is larger than the best PV option (PV0-TES) by a factor of only 1.51 and 1.45 on the 0.1 MW and 10 MW IPH scales, respectively. At all process demands for this case study, PV0-TES and PTC-TES have similar solar fractions (within 5%), meaning that they have similar optimal system designs. Even in this comparison, the f^*_{LCS} value for PTCs is significantly higher than that of PVs. Therefore, the models predict that PTC systems are a better investment than PV systems even with an increase in natural gas costs.

By doubling the natural gas price, the f^*_{LCS} values for PV0-TES are greater than PV1-TES in all scenarios. This result was unexpected because PV1-TES always outperformed PV0-TES with the standard natural gas price in the unconstrained case. However, with higher natural gas prices, optimal solar system designs have much larger aperture areas because it is economically advantageous to reduce natural gas consumption. These larger arrays are capable of meeting the full IPH demand during sunny days (daily inso-

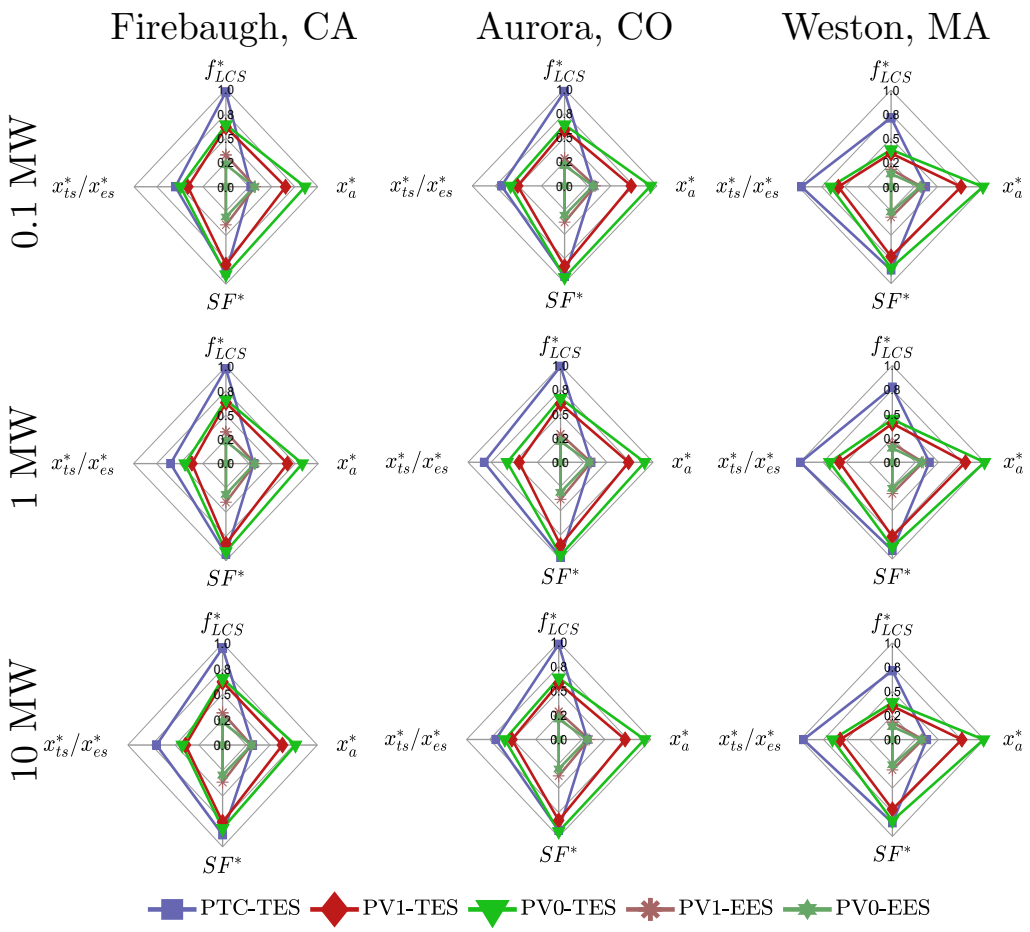

Figure 7: For natural gas priced at \$19.04 per MMBTU, radar plots illustrate the normalized optimal lifecycle cost savings (f^*_{LCS}), aperture area (x^*_a), solar fraction (SF), and thermal energy storage (x^*_{ts}) or electrical energy storage (x^*_{es}) for PTC-TES, PV1-TES, PV0-TES, PV1-EES, PV0-EES systems in three locations and across three process demands. The values were normalized for each process demand using the highest optimal value for each variable. Tabulated results can be found in Table B.1.

lation $\geq$6 kWh/m^2), which, for example, account for more than two-thirds of the Firebaugh TMY data. Under these conditions, energy storage is at capacity, and any excess generation is simply unutilized and lost, regardless of technology. Since PV0-TES and PV1-TES are effectively equal from a pure performance perspective (i.e., both are capable of meeting the process demand), the lower cost of PV0-TES is advantageous, resulting in higher f^*_{LCS} values.

The benefit of PV0 over PV1 only exists when using TES and not EES. In their respective optimal designs, systems with EES have much lower storage capacities and therefore lower SF values than those with TES. On lower solar resource days, EES systems cannot meet the full IPH demand like TES systems, placing a greater importance on the collector's ability to directly meet IPH demands to maximize LCS. Therefore, with EES, PV1 is more favorable than PV0.

An interesting observation regarding all PTC-TES results and the 10 MW PV0-TES results is that the system in Aurora outperforms the equivalent system in Firebaugh. At first glance, this may not seem intuitive considering that Firebaugh has a higher average irradiance throughout the year. However, Aurora's annual irradiance profile complicates the comparison of optimal results. The day-to-day variation in Aurora is broader than in Firebaugh (i.e., there are more cloudy days and more extremely sunny days than in Firebaugh), which means that the system in Aurora must be sized to compensate for the cloudy days. In turn, this also allows for more solar power to be utilized during the sunny days. The higher variation in Aurora also leads to more extremely sunny days. These extremely sunny days generate large surpluses of energy that can be stored and used throughout the night and the following day.

Comparing thermal and electrical storage, thermal storage prevails economically. The optimal LCS values of TES systems are significantly higher than those of EES. The capital cost of EES is so high that other parameters, such as the size of the solar array and the price of natural gas, cannot offset the investment required to implement EES. Overall, increasing the price of natural gas slightly bridges the gap between PTCs and PVs, but the optimal LCS of PTCs is over one million dollars more than that of the PV solutions.

3.5. Future of Photovoltaics

In each of the case studies presented above, PTCs outperform PV options and TES outperforms EES. Despite these findings, the developed models and

optimization-based approach can be used to determine which improvements might be necessary for PVs and EES to match the economic performance of PTCs and TES. This section explores these ideas.

The price of PVs has decreased significantly over the last decade. While PTC technologies have remained stagnant, PVs have had remarkable improvements driven by research and development. According to NREL data [38], PV costs have precipitously decreased: PV0 has fallen by 80% and PV1 has fallen by 82% for large arrays over the last decade. However, the most significant price drops occurred between 2010 and 2018 with a gradual stagnation in later years, as seen in Figure 8.

The developed models allow for the identification of the necessary costs for PVs (PV0 and PV1) to reach economic parity with PTCs for IPH applications. The analysis in this section assumes that the economies of scale remain constant (values of the exponents on x_a and x_{ts}/x_{es}), and only the pre-exponential factor would change in Appendix E. Additionally, this analysis will only consider the most favorable PV technology for each scenario, so as to compare the most applicable PV technology to PTCs. According to the models, for a 10 MW system located in Firebaugh, CA, PVs would require over a 54.0% decrease in cost to be at parity with the f^*_{LCS} value of PTCs (using the natural gas rate of \$9.57/MMBTU). Increasing the price of natural gas increases the economic feasibility of PVs. However, a natural gas price of \$19.04/MMBTU still requires PVs to have a 48% decrease in cost. Therefore, PVs require considerable improvements before they can outperform PTCs in hybridizing IPH systems. Even if the solar industry can meet the price reduction goals set by SETO for 2025 (module cost of \$0.20 per kWh), PV0 and PV1 would only see cost reductions of 22% and 13.7%, respectively [11], falling short of that required for economic parity with PTCs.

Instead of relying on reduced costs, increased efficiency provides an alternative to increasing the economic viability of PVs for IPH applications. If costs remain constant, PVs would require a 125% increase from their current efficiencies to reach parity with PTCs. These increases would require a power conversion efficiency (PCE) of at least 38.4%. With an increased natural gas price of \$19.04/MMBTU, PVs still require a 98% increase in their current efficiency to reach parity with PTCs. This corresponds to a PCE of at least 33.8%. Although efficiencies have been increasing, the most efficient silicon solar cell is significantly below 30%, even under ideal laboratory conditions, as seen in Figure 8. For PVs to be competitive with PTCs, both significant

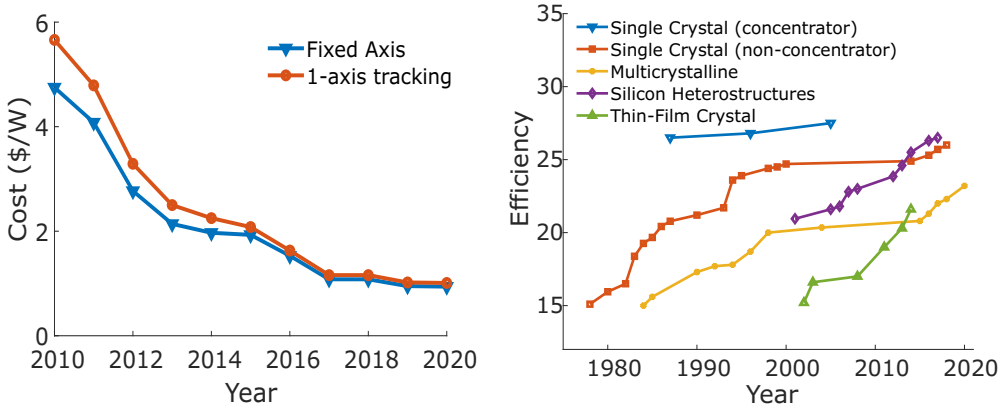

Figure 8: The decreasing costs and increasing efficiency of silicon photovoltaics (PVs) over time. Prices rapidly decreased at the beginning of the decade but have begun to plateau as production is being further optimized. Single crystal (non-concentrating) are the most commonly used PVs for commercial and industrial use but their efficiency has stagnated over the last 20 years, with only a 2% increase in power conversion efficiency.

cost reductions and efficiency increases must be achieved.

Other avenues that enable renewable energy penetration in IPH applications are economic and technological improvements in EES. Lithium-ion batteries are an attractive option because of their currently decreasing costs and increasing performance (e.g. lower material cost and increased charge density) over time [45]. The feasibility of batteries is volatile and changes with technological breakthroughs, but some initial statements can be made using the model developed herein. Similar to the analysis of PV technologies above, if it is assumed that the economies of scale remain constant, then we can assess the conditions for EES to reach economic parity with TES. For this parametric analysis, the capital cost prefactor and physical parameters (e.g., the DoD and round-trip efficiency) of the model were modified.

The findings of this analysis indicate that both cost and physical improvements must be made in tandem to achieve comparable economic feasibility to TES. From a strictly technical performance perspective, increasing the DoD ψ and efficiency η to their highest possible values of 1 is still not enough to become economically competitive with the TES alternative. The optimal results have nearly zero battery storage capacity with only an increase of 0.05% and 0.08% in optimal LCS for PV0-EES and PV1-EES, respectively. This

indicates that the model is not sensitive to technical performance changes alone due to their inability to offset the high capital cost prefactor of EES. On the other hand, from a strictly economic sense, with a $C_{cap,0}$ value of 10 \$/kWh$^{0.94}$ (i.e., a 98% decrease in the EES value of 736.38), PV1-EES achieves parity with PV1-TES within 1.3% and uses a 12-hour Li-ion storage capacity. However, the optimal 0-axis tracking (PV0-EES) configuration results in only 2 hours of battery storage and an LCS value of only 63% of the LCS of the optimal PV0-TES configuration. Although multifaceted improvements in lithium-ion batteries are being made under evolving market conditions, the current technoeconomic analysis indicates that major improvements are necessary before they become a viable option for large scales and applications such as IPH systems.

4. Conclusions

In this article, dynamical models were developed to directly compare the technoeconomic feasibility of different solar technologies for IPH applications. These models apply deterministic global optimization to establish optimal system sizing (array aperture area and energy storage capacity) for each technology. The models account for technology economics, efficiencies, IPH demand/scale, minimum solar fraction, real-world solar performance, variable or constant demand profiles, and natural gas prices to account for a broad scope of hybridization conditions and strategies. While these models were used to provide valid conclusions based on individual case studies, they can also serve as a basis for further customization (i.e., their inputs/parameters adjusted, relaxing assumptions by accounting for additional phenomena) to site-specific information that can help engineering design professionals determine the technoeconomic feasibility of their proposed system.

For hybridized IPH systems, PTCs currently outperform all PV-based technologies regardless of location or process demand. The gap between the technologies shrinks in locations with more sunlight and for larger systems. However, even in the most competitive situation, PTCs are over four times more economically favorable than PVs while providing similar solar fractions. This study identifies that the most competitive PV tracking system depends on the degree of natural gas hybridization. Single-axis tracking (PV1) is more favorable for applications with lower solar fractions, whereas fixed systems (PV0) are more favorable for applications that have higher solar fractions. A parametric study was conducted to identify what necessary improvements

to PVs must be made to reach price parity with PTCs. To reach parity with PTCs, PVs must either have current prices decrease by over 50% at current efficiencies, have their current efficiencies double at current costs, or some combination thereof. Furthermore, PVs using EES are not economically advantageous due to the physical limitations of their efficiency and DoD, as well as impractically high capital costs. The optimization models developed herein were solved to guaranteed global optimality and can also be readily adapted to the changing economic and technological parameters. Therefore, they represent rigorous and flexible models for optimal solar hybridization of IPH systems.

Lastly, the models developed and the rigorous optimization-based approach can help policy makers determine how to allocate subsidies to help achieve Sustainable Development Goal 7, ensuring the availability of sustainable energy. While PV technologies are being thoroughly researched and implemented, PTC technologies are an equally sustainable alternative and can provide thermal energy at a significantly cheaper cost under current economic conditions. As such, decarbonization goals may be achievable for IPH applications without electrification.

Appendix A. Results for Natural Gas Unit Cost of $9.52/MMBTU

Table A.1: The optimal solutions are tabulated for the considered technologies at three process demand sizes. These results were obtained for systems using the US national natural gas average of $9.52 per MMBTU. PTC systems perform significantly better compared to PV systems at lower process demand.

	f^*_{LCS} 10^6 $	x^*_2 m^2	x^*_{ts}/x^*_{es} h	SF^* -	f^*_{LCS} 10^6 $	x^*_2 m^2	x^*_{ts}/x^*_{es} h	SF^* -	f^*_{LCS} 10^6 $	x^*_2 m^2	x^*_{ts}/x^*_{es} h	SF^* -
Firebaugh, CA	0.1 MW				1 MW				10 MW			
PTC-TES	0.0848	419	11.6	0.686	1.06	4,540	12.0	0.711	12.4	49,400	13.0	0.736
PV1-TES	0.00568	577	0.00	0.304	0.145	12,000	10.3	0.628	3.17	123,000	10.6	0.643
PV0-TES	0.00	0.00	0.00	0.00	0.0141	5,650	0.00	0.238	1.45	186,000	13.6	0.782
PV1-EES	0.00488	577	0.00	0.304	0.126	6,060	0.00	0.316	1.99	60,700	0.00	0.317
PV0-EES	0.00	0.00	0.00	0.00	0.00771	5,640	0.00	0.238	0.671	58,600	0.00	0.246
Aurora, CO	0.1 MW				1 MW				10 MW			
PTC-TES	0.0724	509	13.1	0.714	0.969	5,710	14.3	0.759	11.9	61,000	16.0	0.787
PV1-TES	0.00	0.00	0.00	0.00	0.0690	2,790	0.00	0.283	1.90	130,000	10.9	0.626
PV0-TES	0.00	0.00	0.00	0.00	0.00349	5,410	0.00	0.225	1.05	182,000	13.7	0.756
PV1-EES	0.00	0.00	0.00	0.00	0.0626	5,790	0.00	0.283	1.34	60,100	0.0	0.292
PV0-EES	0.00	0.00	0.00	0.00	0.00348	5,360	0.00	0.223	0.546	56,800	0.00	0.235
Weston, MA	0.1 MW				1 MW				10 MW			
PTC-TES	0.0277	467	11.3	0.521	0.504	5,440	13.2	0.579	7.24	65,000	17.9	0.653
PV1-TES	0.00	0.00	0.00	0.00	0.00	0.00	0.00	0.00	0.00	0.00	0.00	0.00
PV0-TES	0.00	0.00	0.00	0.00	0.00	0.00	0.00	0.00	0.00	0.00	0.00	0.00
PV1-EES	0.00	0.00	0.00	0.00	0.00	0.00	0.00	0.00	0.00	0.00	0.00	0.00
PV0-EES	0.00	0.00	0.00	0.00	0.00	0.00	0.00	0.00	0.00	0.00	0.00	0.00

Appendix B. Results for Natural Gas Unit Cost of $19.04/MMBTU

Table B.1: The optimal solutions are tabulated for the considered technologies at three process demans sizes. These results were obtained for systems using a natural gas price of $19.04 per MMBTU. PTCs outperform PVs regardless of process scale. Furthermore, PTCs did not significantly outperform PV technologies at the 0.1 MW process scale.

	f^*_{LCS} 10^6 $	x^*_a m^2	x^*_{ts}/x^*_{es} h	SF^* -	f^*_{LCS} 10^6 $	x^*_a m^2	x^*_{ts}/x^*_{es} h	SF^* -	f^*_{LCS} 10^6 $	x^*_a m^2	x^*_{ts}/x^*_{es} h	SF^* -
Firebaugh, CA	0.1 MW				1 MW				10 MW			
PTC-TES	0.302	620	15.6	0.796	3.33	7,230	20.4	0.841	36.2	82,400	26.52	0.880
PV1-TES	0.192	1,490	12.0	0.732	2.15	15,400	12.5	0.735	23.7	167,000	15.7	0.767
PV0-TES	0.200	1,960	14.3	0.812	2.26	19,700	15.0	0.815	25.0	198,000	16.2	0.820
PV1-EES	0.102	727	0.00	0.353	1.11	7,540	0.00	0.359	12.0	78,300	0.00	0.365
PV0-EES	0.0703	709	0.00	0.280	0.785	7,400	0.00	0.287	8.62	78,800	0.00	0.296
Aurora, CO	0.1 MW				1 MW				10 MW			
PTC-TES	0.303	713	19.8	0.841	3.37	7,920	28.0	0.885	37.0	90,300	35.4	0.929
PV1-TES	0.181	1,650	14.9	0.750	2.08	17,500	15.1	0.772	23.3	183,000	16.8	0.792
PV0-TES	0.198	2,120	17.0	0.851	2.27	21,600	19.7	0.865	25.4	220,000	21.6	0.877
PV1-EES	0.0891	754	0.00	0.338	0.992	7,880	0.00	0.346	10.9	81,600	0.00	0.351
PV0-EES	0.0664	706	0.00	0.273	0.746	7,450	0.00	0.281	8.25	79,800	0.00	0.291
Weston, MA	0.1 MW				1 MW				10 MW			
PTC-TES	0.221	861	28.1	0.774	2.63	9,660	33.8	0.820	30.2	105,000	37.6	0.849
PV1-TES	0.110	1,750	16.3	0.653	1.38	18,800	19.4	0.691	16.6	202,000	23.5	0.726
PV0-TES	0.122	2,260	18.94	0.754	1.53	23,700	23.1	0.787	18.4	248,000	25.9	0.812
PV1-EES	0.0570	756	0.00	0.283	0.672	7,970	0.00	0.293	7.69	83,700	0.00	0.301
PV0-EES	0.0423	722	0.00	0.235	0.507	7,600	0.00	0.243	5.86	80,100	0.00	0.251

Appendix C. Modeling Parameters

Name	Value	Units	Description
I_{sc}	6.23	A	Short circuit current
α_T	0.035	-	Temperature coefficient for current
q	1.602×10^{-19}	C	Electric charge
V_{oc}	64.8	V	Open circuit voltage
k_B	1.38×10^{-23}	J/K	Boltzmann constant
N	96	Cells	Number of cells in series
E_{g0}	1.17	eV	Band gap energy at 0K
α	4.73×10^{-4}	eV/K^2	Electron–phonon pair constant
β	636	K	Parameter related to Debye Temperature
V_{mp}	54.8	V	Maximum power voltage
I_{mp}	5.86	A	Maximum power current
ϵ_r	0.985	-	Reflection efficiency
ϵ_s	0.95	-	Soiling efficiency
ϵ_i	0.97	-	Inverter efficiency
ϵ_w	0.99	-	Wiring efficiency
η	0.85	-	Li-ion battery round-trip efficiency
ψ	0.8	-	Li-ion battery depth of discharge

Appendix D. Photovoltaic Modeling

Appendix D.1. Photovoltaic Equations

$$I_{ph} = [I_{sc} + \alpha_T(T_c - T_r)]\frac{G}{G_r} \tag{D.1}$$

$$I_0 = \frac{I_{sc}}{\exp\left(\frac{qV_{oc}}{nk_BNT_c}\right) - 1}\left(\frac{T_c}{T_r}\right)^3 \exp\left(\frac{qE_g(\frac{1}{T_r} - \frac{1}{T_c})}{nk_B}\right) \tag{D.2}$$

$$E_g = E_{g0} - \frac{\alpha T^2}{T + \beta} \tag{D.3}$$

$$R_s = \frac{\frac{N_s n k_B T_c}{q}\log(1 - \frac{I_{mp}}{I_{sc}}) + V_{oc} - V_{mp}}{I_{mp}} \tag{D.4}$$

$$n = \frac{q(2V_{mp} - V_{oc})}{Nk_BT_r(\frac{I_{mp}}{I_{sc}-I_{mp}} + \log(\frac{I_{sc}-I_{mp}}{I_{sc}}))} \tag{D.5}$$

Appendix D.2. Solar Time Factors and Angles

Earth's orbital velocity is not constant throughout the year and so we must account for the variations between the apparent solar time AST and the local clock time with the function ET, which is a function of the day of the year N:

$$B = (N - 81)\frac{360}{365}, \tag{D.6}$$

$$ET = 9.87\sin 2B - 7.53\cos B - 1.5\sin B. \tag{D.7}$$

With this correction, the apparent solar time AST is calculated as

$$AST = ET \pm 4(15[\text{Time Zone (h)}] - [\text{Longitude}^\circ]), \tag{D.8}$$

where the $(+)$ is chosen if the location is east of the prime meridian and $(-)$ if it is to the west. In addition to these solar time factors, solar angles must be calculated to model the performance of the solar technologies.

The declination angle δ, hour angle γ, zenith angle ϕ, and solar elevation angle α, are calculated by:

$$\delta = 23.45^\circ \sin B, \tag{D.9}$$

$$\gamma = 15\left(\mathrm{h} + \frac{AST}{60} - 12\right), \tag{D.10}$$

$$\cos\phi = \sin\left[\text{Latitude}^\circ\right]\sin\delta + \cos\left[\text{Latitude}^\circ\right]\cos\delta\cos\gamma, \tag{D.11}$$

$$\sin\alpha = \cos\phi. \tag{D.12}$$

Finally, the azimuth ζ is calculated by:

$$\zeta = \begin{cases} \arcsin\left(\frac{\cos\delta\sin\gamma}{\cos\alpha}\right), & \text{if } \cos\gamma > \frac{\tan\delta}{\tan\left[\text{Latitude}^\circ\right]}, \\ \left|\arcsin\left(\frac{\cos\delta\sin\gamma}{\cos\alpha}\right)\right| - \pi, & \text{elseif } \cos\gamma \le \frac{\tan\delta}{\tan\left[\text{Latitude}^\circ\right]} \wedge \gamma \le 0, \\ \pi - \arcsin\left(\frac{\cos\delta\sin\gamma}{\cos\alpha}\right), & \text{else,} \end{cases} \tag{D.13}$$

where the first case holds if the sun rises/sets south of the E-W line, and the other two cases are when the sun rises/sets north of the E-W line.

Appendix D.3. Zero-Axis Tracking

For the zero-axis tracking model, the surface tilt angle is set equal to the latitude. Under this condition, the incident angle θ is calculated by:

$$\cos\theta = \cos\delta\cos\gamma. \tag{D.14}$$

Appendix D.4. One-Axis Tracking

For the one-axis tracking model, systems are fixed in the N-S orientation and track the sun east to west with no tilt from the horizontal plane in the N-S direction. The surface incident angle θ for the one-axis tracking system is calculated by

$$\cos\theta = \sqrt{\cos^2\phi + \cos^2\delta\sin^2\gamma}. \tag{D.15}$$

Appendix E. Cost Parameters

$C_{PV0,0}$, specific installed cost of PV0 ($/m$^{1.92}$)	200.18
$C_{PV1,0}$, specific installed cost of PV1 ($/m$^{1.92}$)	223.49
$C_{PTC,0}$, specific installed cost of PTC ($/m$^{1.84}$)	425
$C_{EES,0}$, capital cost of Lithium-ion battery ($/kWh$_{\mathrm{e}}^{0.94}$)	736
$C_{TES,0}$, capital cost of thermal energy storage ($/kWh$_{\mathrm{th}}^{0.91}$)	45.14
natural gas cost ($/MMBTU)	9.52

Data Availability

Data and source code used in this study are available on the GitHub repository: https://github.com/PSORLab/SolarIPH.

References

[1] U.S. energy consumption by source and sector, Technical Report, Energy Information Administration, 2019. https://www.eia.gov/energyexplained/us-energy-facts/, Accessed 2021-08-19.

[2] Industrial Sector Energy Consumptions, Technical Report, Energy Information Administration, 2021. https://www.eia.gov/totalenergy/data/monthly/pdf/sec2_9.pdf, Accessed 2021-08-19.

[3] R. Margolis, C. McMillan, P. Kurup, Solar for Industrial Process Heat, Technical Report, U.S. Department of Energy, 2019. https://www.energy.gov/sites/prod/files/2019/04/f61/CSP%20Summit2019%20NREL%20Margolis%20SIPH.pdf, Accessed 2021-09-19.

[4] C. A. Schoeneberger, C. A. McMillan, P. Kurup, S. Akar, R. Margolis, E. Masanet, Solar for industrial process heat: A review of technologies, analysis approaches, and potential applications in the united states, Energy 206 (2020) 118083. doi:doi:10.1016/j.energy.2020.118083.

[5] A. Hasanbeigi, L. A. Kirshbaum, B. Collison, D. Gardiner, Electrfying U.S. Industry: A Technology and Process-Based Approach to Decarbonization, Technical Report, Renewable Thermal Collaborative, 2021. https://www.renewablethermal.org/wp-content/uploads/2018/06/Electrifying-U.S.-Industry-6.8.21.pdf, Accessed 2022-06-09.

[6] R. Gold, Status report on electrification policy: Where to next?, Current Sustainable/Renewable Energy Reports 8 (2021) 114–122. doi:doi:10.1007/s40518-021-00180-w.

[7] World Energy Balances, Technical Report, IEA, 2021. https://www.iea.org/data-and-statistics/data-sets, Accessed 2022-28-11.

[8] S. Madeddu, F. Ueckerdt, M. Pehl, J. Peterseim, M. Lord, K. A. Kumar, C. Krüger, G. Luderer, The CO_2 reduction potential for the European industry via direct electrification of heat supply (power-to-heat), Environmental Research Letters 15 (2020) 124004. doi:doi:10.1088/1748-9326/abbd02.

[9] J. Deason, M. Wei, G. Leventis, S. Smith, L. Schwartz, Electrification of buildings and industry in the United States: Drivers, barriers, prospects,and policy approaches, Technical Report, Lawrence Berkeley National Laboratory, 2018. https://eta-publications.lbl.gov/sites/default/files/electrification_of_buildings_and_industry_final_0.pdf, Accessed 2022-07-13.

[10] U. Pillai, Drivers of cost reduction in solar photovoltaics, Energy Economics 50 (2015) 286–293. doi:doi:10.1016/j.eneco.2015.05.015.

[11] T. J. Silverman, H. Huang, Solar Energy Technologies Office Multi-Year Program Plan, Technical Report, Office of Energy Efficiency & Renewable Energy, 2021. https://www.energy.gov/sites/default/files/2021-06/Solar%20Energy%20Technologies%20Office%202021%20Multi-Year%20Program%20Plan%2006-21.pdf, Accessed 2022-06-06.

[12] G. Kavlak, J. McNerney, J. E. Trancik, Evaluating the causes of cost reduction in photovoltaic modules, Energy Policy 123 (2018) 700–710. doi:doi:10.1016/j.enpol.2018.08.015.

[13] H. Son, M. Kim, J.-K. Kim, Sustainable process integration of electrification technologies with industrial energy systems, Energy 239 (2022) 122060. doi:doi:10.1016/j.energy.2021.122060.

[14] Small Innovative Projects in Solar 2022, Technical Report, US Department of Energy, 2022.

[15] G. Manikandan, S. Iniyan, R. Goic, Enhancing the optical and thermal efficiency of a parabolic trough collector – a review, Applied Energy 235 (2019) 1524–1540. doi:doi:10.1016/j.apenergy.2018.11.048.

[16] V. Jebasingh, G. J. Herbert, A review of solar parabolic trough collector, Renewable and Sustainable Energy Reviews 54 (2016) 1085–1091. doi:doi:10.1016/j.rser.2015.10.043.

[17] M. Stuber, A differentiable model for optimizing hybridization of industrial process heat systems with concentrating solar thermal power, Processes 6 (2018) 76. doi:doi:10.3390/pr6070076.

[18] U.S. Price of Natural Gas Sold to Commercial Consumers, Technical Report, U.S. Energy Information Administration, 2022. https://www.eia.gov/dnav/ng/hist/n3020us3m.htm, Accessed 2021-07-14.

[19] K. M. Powell, J. D. Hedengren, T. F. Edgar, Dynamic optimization of a hybrid solar thermal and fossil fuel system, Solar Energy 108 (2014) 210–218. doi:doi:10.1016/j.solener.2014.07.004.

[20] A. Wächter, Biegler, On the implementation of an interior-point filter line-search algorithm for large-scale nonlinear programming, Mathematical Programming 106 (2006) 25–57. doi:doi:10.1007/s10107-004-0559-y.

[21] A. Allouhi, Y. Agrouaz, M. B. Amine, S. Rehman, M. Buker, T. Kousksou, A. Jamil, A. Benbassou, Design optimization of a multi-temperature solar thermal heating system for an industrial process, Applied Energy 206 (2017) 382–392. doi:doi:10.1016/j.apenergy.2017.08.196.

[22] S. Scolan, S. Serra, S. Sochard, P. Delmas, J.-M. Reneaume, Dynamic optimization of the operation of a solar thermal plant, Solar Energy 198 (2020) 643–657. doi:doi:10.1016/j.solener.2020.01.076.

[23] GAMS Development Corporation, General Algebraic Modeling System (GAMS), Technical Report, Fairfax, VA, USA, 2021.

[24] A. S. Drud, CONOPT—a large-scale GRG code, ORSA Journal on Computing 6 (1994) 207–216. doi:doi:10.1287/ijoc.6.2.207.

[25] J. Immonen, K. M. Powell, Dynamic optimization with flexible heat integration of a solar parabolic trough collector plant with thermal energy storage used for industrial process heat, Energy Conversion and Management 267 (2022) 115921. doi:doi:10.1016/j.enconman.2022.115921.

[26] F. van den Bergh, A. P. Engelbrecht, A convergence proof for the particle swarm optimiser, Fundamenta Informaticae 105 (2010) 341–374. doi:doi:10.3233/fi-2010-370.

[27] S. Meyers, B. Schmitt, K. Vajen, Renewable process heat from solar thermal and photovoltaics: The development and application of a universal methodology to determine the more economical technology, Applied Energy 212 (2018) 1537–1552. doi:doi:10.1016/j.apenergy.2017.12.064.

[28] O. B. Mousa, R. A. Taylor, A. Shirazi, Multi-objective optimization of solar photovoltaic and solar thermal collectors for industrial rooftop applications, Energy Conversion and Management 195 (2019) 392–408. doi:doi:10.1016/j.enconman.2019.05.012.

[29] L. Magnier, F. Haghighat, Multiobjective optimization of building design using TRNSYS simulations, genetic algorithm, and artificial neural network, Building and Environment 45 (2010) 739–746. doi:doi:10.1016/j.buildenv.2009.08.016.

[30] M. Wetter, GenOpt - A generic optimization program, 2001. http://www.ibpsa.org/proceedings/BS2001/BS01_0601_608.pdf, Accessed 2023-11-03.

[31] M. E. Wilhelm, M. D. Stuber, EAGO.jl: Easy advanced global optimization in Julia, Optimization Methods and Software 37 (2022) 425–450. doi:doi:10.1080/10556788.2020.1786566.

[32] A. Sidibba, D. Ndiaye, M. E. Bah, S. Bouhamady, Analytical modeling and determination of the characteristic parameters of the different commercial technologies of photovoltaic modules, Journal of Power and Energy Engineering 06 (2018) 14–27. doi:doi:10.4236/jpee.2018.63002.

[33] National Renewable Energy Laboratory, National solar radiation database (NSRDB), 2022. URL: https://nsrdb.nrel.gov/nsrdb-viewer, NSRDB: National Solar Radiation Database.

[34] E. Mboumboue, D. Njomo, Mathematical modeling and digital simulation of PV solar panel using MATLAB software, International Journal of Emerging Technology and Advanced Engineering 3 (2013).

[35] System Advisor Model Version 2020.11.29 (SAM 2020.11.29), Technical Report, National Renewable Energy Laboratory, 2020. https://sam.nrel.gov/, Accessed 2021-09-10.

[36] S. A. Kalogirou, Solar Energy Engineering Processes and Systems, second ed., Academic Press, Boston, 2014. doi:doi:10.1016/C2011-0-07038-2.

[37] M. Schimpe, M. Naumann, N. Truong, H. C. Hesse, S. Santhanagopalan, A. Saxon, A. Jossen, Energy efficiency evaluation of a stationary lithium-ion battery container storage system via electro-thermal modeling and detailed component analysis, Applied Energy 210 (2018) 211–229. doi:doi:10.1016/j.apenergy.2017.10.129.

[38] D. Feldman, V. Ramsamy, R. Fu, A. Ramdas, J. Desai, R. Margolis, U.S. Solar Photovoltaic System and Energy Storage Cost Benchmark: Q1 2020, Technical Report, National Renewable Energy Laboratory, 2021. https://www.nrel.gov/docs/fy21osti/77324.pdf, Accessed 2022-05-19.

[39] R. Fu, T. Remo, R. Margolis, 2018 U.S. Utility-Scale Photovoltaics Plus-Energy Storage System Costs Benchmark, Technical Report, National Renewable Energy Laboratory, https://www.nrel.gov/docs/fy19osti/71714.pdf, 2018.

[40] K. Ardani, E. O'Shaughnessy, R. Fu, C. McClurg, J. Huneycutt, R. Margolis, Installed Cost Benchmarks and Deployment Barriers for Residential Solar Photovoltaics with Energy Storage: Q1 2016, Technical Report, National Renewable Energy Laboratory, Rocky Mountain Institute, U.S. Department of Energy, https://www.nrel.gov/docs/fy17osti/67474.pdf, 2016.

[41] N. DiOrio, A. Dobos, , S. Janzou, Economic Analysis Case Studies of Battery Energy Storage with SAM, Technical Report, National Renewable Energy Laboratory, 2015. https://www.nrel.gov/docs/fy16osti/64987.pdf.

[42] J. McLaren, P. Gagnon, K. Anderson, E. Elgqvist, R. Fu, T. Remo, Battery Energy Storage Market: Commercial Scale, Lithium-ion Projects

in the U.S., Technical Report, National Renewable Energy Laboratory, 2016. https://www.nrel.gov/docs/fy17osti/67235.pdf.

[43] J. Bezanson, A. Edelman, S. Karpinski, V. B. Shah, Julia: A fresh approach to numerical computing, SIAM Review 59 (2017) 65–98. doi:doi:10.1137/141000671.

[44] I. Dunning, J. Huchette, M. Lubin, JuMP: A modeling language for mathematical optimization, SIAM Review 59 (2017) 295–320. doi:doi:10.1137/15M1020575.

[45] M. S. Ziegler, J. Song, J. E. Trancik, Determinants of lithium-ion battery technology cost decline, Energy & Environmental Science 14 (2021) 6074–6098. doi:doi:10.1039/d1ee01313k.